ALL THINGS LIGHTING® ASSOCIATION

2016 Annual Review

View this journal at
https://www.allthingslighting.org/publications

ISSN 2816-7848

ALL THINGS LIGHTING® ASSOCIATION

Contributor- Ian Ashdown, Senior Scientist

CONTENTS

ALL THINGS LIGHTING

View this journal at https://www.allthingslighting.org/publications

  ISSN 2816-7848

ARCHITECTURAL INFORMATION

SPORTS LIGHTING REGULATIONS

Ian Ashdown, P. Eng., FIES, Senior Scientist, SunTracker Technologies Ltd. Published: 2016/04/30

This blog article has a somewhat frustrating history. About a year ago, I was asked to volunteer my time to write a primer of light and color as it relates to sports lighting regulations. I was told the name of the organization I was volunteering my time for, but I did not pay much attention — it seemed like a good cause.

I should have perhaps paid more attention before agreeing to volunteer — the Green Sports Alliance is not the poorest of socially responsible organizations.

Upon completing the primer, I was told that it was far too technical for its intended audience. Hopefully, you as my readers will disagree.

Sports Lighting Requirements

Sports lighting has specific requirements that may not be familiar to many lighting designers. The Illuminating Engineering Society publishes detailed recommendations related to sports lighting (IES 2009, 2010a, 2015), while various professional sports organizations have their own specific requirements (for example, FIFA 2007, FIH 2011, NCAA 2010a and 2010b, and Lewis and Brill 2013).

Illuminance

In sports lighting, there are two forms of illuminance measurements that are of interest: *HORIZONTAL* illuminance and *VERTICAL* illuminance.

Horizontal illuminance is typically measured on a horizontally oriented imaginary surface one meter (~3 feet) above the field surface. Multiple measurements are usually measured (or calculated during the lighting design phase) on a grid. The National Football League, for example (Lewis and Brill 2013), specifies a grid spacing of 5 meters (~16 feet).

Vertical illuminance is measured on a vertically oriented imaginary surface. Unlike horizontal illuminance, both the position and orientation of the vertical surface must be specified. To understand why, consider a vertical surface illuminated by a single light source (FIG. 1).

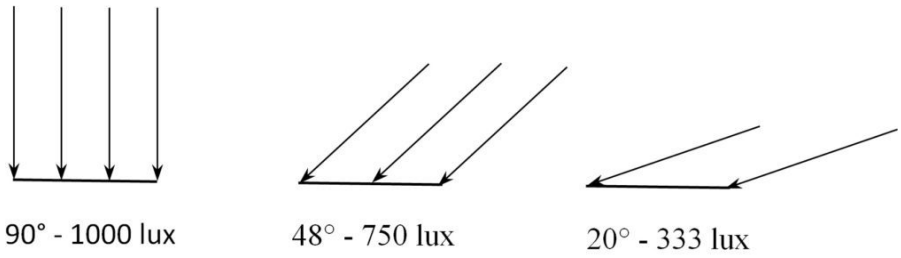

FIG. 1 – Illuminance of surface depends on angle of illumination.

As the angle of illumination decreases, the lumens per square meter decrease as well, until at grazing angles the surface is barely illuminated at. This can clearly be seen with a sphere illuminated by a single light source (FIG. 2).

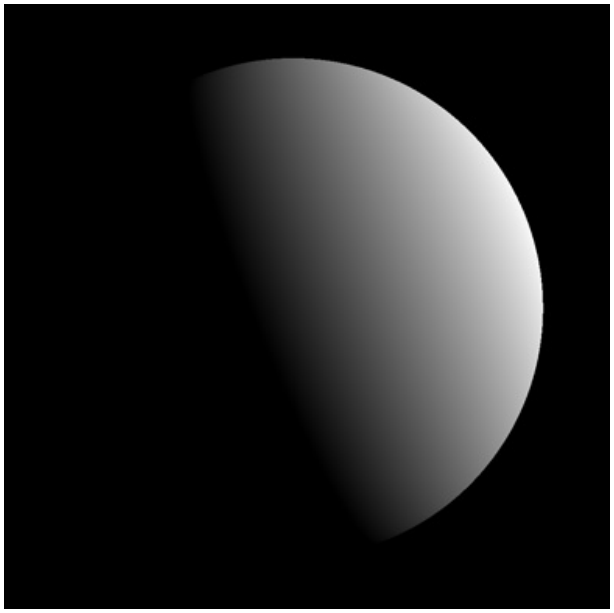

FIG. 2 – Sphere illuminated by a single distant light source.

In practice, there will be multiple luminaires illuminating the field, each of which will contribute to the illumination of a vertical surface — such as a player's face. It is therefore important to ensure that the vertical illuminance is within minimum and maximum limits so that the players' faces and team numbers can always be seen.

With this in mind, the "falloff" in illuminance with distance from a single luminaire must also be kept in mind. As shown in FIG. 3, a light source **S** illuminates two imaginary surfaces, the first one at distance **d** from the light source, and the second at twice the distance. Both surfaces receive the same amount of light (lumens) from **S**, but the area of the second surface is four times that of the first. Consequently, its illuminance (lumens per square meter) is only one-quarter that of the first surface.

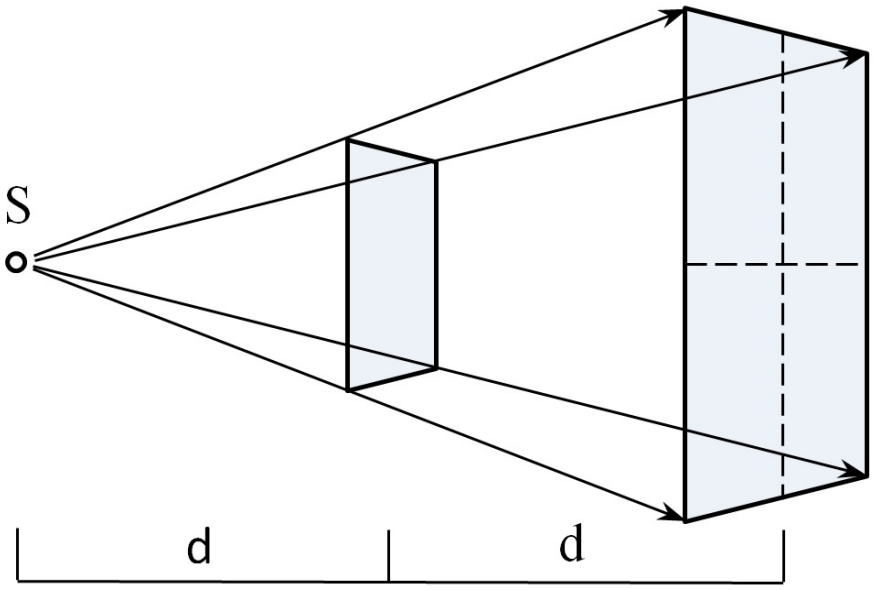

FIG. 3 – Inverse Square Law.

Generalizing this to any distance, it is easy to see that the illuminance from a single luminaire will decrease, or "fall off," according to the square of the distance. This is the basis of the *INVERSE SQUARE LAW* used by lighting designers.

Finally, "TV illuminance" is occasionally used for television broadcasting purposes (IES 2015). It is the illuminance measured at a position on the playing field when the illuminance meter is aimed directly at a specified camera position. In practice, of course, multiple luminaires are used to (more or less) evenly illuminate a playing field.

Uniformity

Uniformity of illumination is important for sports. It enables both the players and the spectators to easily follow the action, and it provides consistent lighting for the television cameras and photographers. Sports field lighting for internationally televised events must meet exacting standards, while more leeway is generally allowed for other events.

There are three measures (or more properly *METRICS*) used to specify the desired uniformity of horizontal and vertical illuminance on the playing field. The simplest metric is the maximum-to-minimum ratio, commonly referred to as the *UNIFORMITY RATIO*. Using NFL requirements as an example, horizontal illuminance is designated Eh, and so the uniformity ratio is expressed as Eh_{max}/Eh_{min}. Using a measurement grid for the playing field with 5-meter spacing, this ratio for all measurement values must be 1.4:1 or less.

Again using the NFL requirements, vertical illuminance is designated Ev, and the uniformity ratio Ev_{max}/Ev_{min} must also be 1.4:1 or less.

The NFL requirements go further in specifying that: 1) the ratio of the average horizontal illuminance $Eh_{avg}$to average vertical illuminance Ev_{avg} as seen from camera #1 (that is, with each vertical surface

facing the camera) must be between 1.0 and 2.0, with a target value of 1.5; 2) the ratio of vertical illuminances at any point on the field between the four imaginary vertical surfaces facing the four sides of the field shall be between 0.6 and 0.9; and 3) the average vertical illuminance Ev_{avg} facing towards camera #1 shall not be less that Ev_{avg} for the other three orthogonal (that is, right-angle) orientations. In other words, it can get complicated.

The second uniformity metric is the *COEFFICIENT OF VARIATION*, designated CV. Without delving into the mathematics of this statistical value, it can be likened to the point spread in sports betting. (If you must know the details, the equation is:

$$CV = \frac{\sqrt{\frac{\sum_{i=1}^{n}(x_i - \bar{x})^2}{n}}}{\bar{x}}$$

with details left to the interested reader — see [IES 2009, 2015].) It is basically a measure of how "smooth" the lighting distribution is across the playing field.

The third metric is the *UNIFORMITY GRADIENT*, designated UG. It is defined as the ratio between illuminance values between adjacent measuring points on a square grid. Whereas CV describes the average non-uniformity for the entire field, UG describes the maximum non-uniformity. It is particularly important in sports with fast-moving balls and the like, as changes in illuminance can make it more difficult to judge their speed.

Visual Glare

Visual *GLARE* occurs when the luminance of the luminaires within the observerís field of view (either a player or spectator) is sufficiently greater than the average luminance to which the observerís eye have adapted. It may cause visual discomfort (in response to which we tend to squint), or it may impair the vision of objects and details (such as past-moving balls and the like).

As a psychophysiological phenomenon, glare is both literally and figuratively "in the eye of the beholder." All lighting researchers can do is present subjects in a laboratory with a lighting setup and ask them to rate the glare on a subjective scale. While it cannot be directly measured in the field, a glare rating metric, designated GR, can be calculated (typically at the design phase) in accordance with CIE 112-1994, *GLARE EVALUATION SYSTEM FOR USE WITH OUTDOOR SPORTS AND AREA LIGHTING* (CIE 1994).

Central to these calculations are five parameters:

1. The luminance's of the luminaires as seen by the observer;
2. The angular extent of the luminaires in the observer's field of view;
3. The position of the luminaires in the observer's field of view relative to the line of sight;
4. The number of luminaires in the observer's field of view; and
5. The average luminance of the observer's entire field of view.

It is important to note that the GR metric depends on where the observer is positioned relative to the luminaires, and the line-of-sight direction. Consequently, any GR requirements must specify these parameters. The NFL requirements, for example, require that GR be less than 40 for all main cameras (Lewis and Brill 2013).

Color

Many sports organizations specify the allowable *CORRELATED COLOR TEMPERATURE*, designated CCT, for sports field lighting. For example:

Organization	CCT
FIFA	= 4000K
FIH	> 4000K
NCAA	> 3600K
NFL	5600K (alternatively 5000K to 7000K)

where the symbol 'K' represents *KELVINS* (where one kelvin is equal to one degree Celsius).
To put these numbers into context, quartz halogen and warm white LED lamps typically have CCTs of approximately 3000K, metal halide lamps typically have CCTs of 4000K, and daylight LED lamps typically have CCTs of 5000K.

FIG. 4 – Light source correlated color temperatures.

Our eyes adapt quite well to light sources with different CCTs, ranging from 2700K for 100-watt incandescent lamps to 10000K for the blue sky. Even though the light itself may look colored (FIG. 8), objects seen under these light sources appear to have approximately the same colors, with whites looking white.

The same is not true with television and digital cameras, however, which must be adjusted (*COLOR-BALANCED*) to display the colors we expect to see. This is why it is important that all the luminaires in a sports lighting installation have approximately the same CCT. If they do not, the television cameras will display annoying color shifts as they pan across the field.

Many sports organizations also specify the minimum allowable *COLOR RENDERING INDEX*, designated CRI, for sports lighting. For example:

Organization	CRI R_a
FIFA	= 65
FIH	> 65
NCAA	> 65
NFL	= 90

where the CRI R_a metric is a measure of the average color shift of various colors viewed under the light source when compared to viewing the colors under an incandescent or daylight source with the same CCT. A detailed explanation of color rendering is beyond the scope of this introductory chapter, but the topic is fully explained in CIE 13.3-1995, *METHOD OF MEASURING AND SPECIFYING COLOUR RENDERING PROPERTIES OF LIGHT SOURCES* (CIE 1995).

In general, a minimum CRI of 65 is merely adequate, and is representative of what could be achieved with high-wattage metal halide lamps. With today's solid-state lighting, a minimum CRI of 80 or greater is common, and CRIs of 90 and above are preferred.

It must also be emphasized that R_a metric represents the average color shift. Solid-state lighting products may also specify a CRI R_9 metric, which represents the color shift specifically for red colors. A high R_9 value is desirable, especially where team outfits feature saturated red colors.

In terms of television broadcast cameras, a more appropriate color rendering metric is the Television Lighting Consistency Index TLCI-2012 (EBU 2014). Like the CRI R_a metric, this is a measure of the average color shift of various colors viewed under the light source; the difference is that the observer is a color television camera rather than a human.

Spectrally Enhanced Lighting

There is some interest in the topic of *SPECTRALLY ENHANCED LIGHTING* for sports field applications. For some visually demanding tasks, the recommended illuminance values can be reduced through the use of light sources with high blue content. A full discussion is presented in IES TM-24-13, *AN OPTIONAL METHOD FOR ADJUSTING THE RECOMMENDED ILLUMINANCE FOR VISUALLY DEMANDING TASKS WITHIN IES ILLUMINANCE CATEGORIES P THROUGH Y BASED ON LIGHT SOURCE SPECTRUM* (IES 2013).

It could be argued TM-24-13 can be applied to sports lighting, as it defines (p. 3) "visually demanding tasks" as "… tasks that are based on the ability to discern visual detail to ensure speed and/or accuracy." In this situation, "visual detail" could be interpreted as a fast-moving ball or hockey puck. Furthering the argument, TM-24-13 applies to illuminance categories P through Y, which the *IES LIGHTING HANDBOOK, 10TH EDITION* (IES 2010a) defines in Table 4.1, *RECOMMENDED ILLUMINANCE*

TARGETS, as interior and exterior lighting installations where the illuminance targets are in excess of 300 lux. Categories P (average 300 lux) through W (average 3000 lux) specifically include "some sports situations" (without defining them).

There are several problems, however. The first is that most sports organizations specify minimum horizontal and vertical illuminances without taking spectrally enhanced lighting into account. Any sports lighting that reduced these values based on TM-24-13 would not be in compliance with these specifications.

The second problem is that the recommended illuminance targets for sports lighting involving television broadcasting are based on the minimum illuminance requirements of the television cameras. These are of course independent of the human visual system, and so the reduced illuminance values calculated in accordance with TM-24-13 do not apply.

The third problem is the most crucial: the Illuminating Engineering Society issued a lengthy position statement (included in TM-24-13) that unequivocally states (in boldface type), "TM-24 should not be used for the development of energy policy or energy efficiency programs purposes for any lighting applications, as this goes against current IES recommendations."

Light Pollution

Outdoor lighting illuminates not only objects on the ground, but the overhead sky as well. The International Dark-Sky Association reminds us that this unintentional light pollution threatens professional and amateur astronomy, disrupts nocturnal ecosystems, affects circadian rhythms of both humans and animals, and wastes over two billion dollars of electrical energy per year in the United States alone.

It might seem obvious that sports field lighting is a major contributor to light pollution, but this is true only in a local sense. According to a US Department of Energy study (DOE 2010), stadium lighting contributes a maximum of 6 percent (compared to 48 percent for roadway lighting and 34 percent for parking lot lighting) on a national scale. (This further assumes that the stadium lighting is always on at night.)

Outdoor Lighting	Percent Lumens
Roadway	48
Parking	34
Building exteriors	10
Stadiums	6
Billboards	1
Traffic signals	1

On a local scale, however, light pollution from stadiums and sports fields can be a concern, particularly for surrounding residential neighborhoods. This includes not only light that is reflected from the ground and illuminates the sky overhead, but also light trespass and glare from improperly shielded luminaires.

IES TM-15-11, *LUMINAIRE CLASSIFICATION SYSTEM FOR OUTDOOR LUMINAIRES* (IES 2011a) and the *JOINT IDA-IES MODEL LIGHTING ORDINANCE (MLO) WITH USER'S GUIDE* (IES 2011b) provide detailed information on designing outdoor lighting systems that minimize unintended light pollution.

References

CIE. 1994. CIE 112-1994, Glare Evaluation System for Use within Outdoor Sports and Area Lighting.

Vienna, Austria: Commission International de l'Eclairage.

CIE. 1995. CIE 13.3-1995, Method of Measuring and Specifying Colour Rendering Properties of Light Sources. Vienna, Austria: Commission International de l'Eclairage.

DOE. 2010. 2010 U.S. Lighting Market Characterization, U.S. Department of Energy Building Technologies Program.

EBU. 2014. Tech 3355, Method for the Assessment of the Colorimetric Properties of Luminaires: The Television Lighting Consistency Index (TLCI-2012) and the Television Luminaire Matching Factor (TLMF-2013. Geneva, Switzerland: European Broadcast Union.

FIFA. 2007. Football Stadiums: Technical Recommendations and Requirements, 4th Edition. Zurich, Switzerland: FÈdÈration Internationale de Football Association.

FIH. 2011. Guide to the Artificial Lighting of Hockey Pitches, 6th Edition. Lausanne, Switzerland: International Hockey Federation.

IES. 2009. IES RP-6-09, Recommended Practice for Sports and Recreational Area Lighting. New York, NY: Illuminating Engineering Society.

IES. 2010a. IES Lighting Handbook, 10th Edition. New York, NY: Illuminating Engineering Society.

IES. 2011a. IES TM-15-11, Luminaire Classification System for Outdoor Luminaires. New York, NY: Illuminating Engineering Society.

IES. 2011b. Joint IDA-IES Model Lighting Ordinance (MLO) with Userís Guide. New York, NY: Illuminating Engineering Society.

IES. 2013. IES TM-24-13, An Optional Method for Adjusting the Recommended Illuminance for Visually Demanding Tasks Within IES Illuminance Categories P through Y Based on Light Source Spectrum. New York, NY: Illuminating Engineering Society.

IES. 2015. IES RP-6-15, Sports and Recreational Area Lighting. New York, NY: Illuminating Engineering Society.

Lewis, D., and S. Brill. 2013. Broadcast Lighting: NFL Stadium Lighting. The Design Lighting Group Inc.

NCAA. 2010a. NCAA Basketball Championships Best Lighting Practices. National Collegiate Athletic Association.

NCAA. 2010b. NCAA Best Lighting Practices. National Collegiate Athletic Association.

Appendix A

A.1. What is Light?

A primer on sports lighting must answer the obvious question: what is light? The Oxford English Dictionary, the pre-eminent dictionary of the English language, describes light rather loosely as, “the natural agent that stimulates the sense of sight.” More technically, light is *ELECTROMAGNETIC RADIATION*.

What we see as visible light is only a tiny fraction of the electromagnetic *SPECTRUM*, extending from very low-frequency radio waves through microwaves, infrared, visible light, and ultraviolet to x-rays and ultra-energetic gamma rays. Our eyes respond to visible light; detecting the rest of the electromagnetic spectrum requires an arsenal of scientific instruments ranging from radio receivers to scintillation counters.

Our interest however is solely in visible light — it is what we see when we look at the world.

A.2. Quantifying Light

We can think of light as massless subatomic particles called *PHOTONS*. They are emitted by light sources such as metal halide lamps and light-emitting diodes (LEDs), and travel through space until they encounter physical objects. They may then be reflected, refracted, scattered, or absorbed. Some of those photons will intersect our eyes, enabling us to see (FIG. A1).

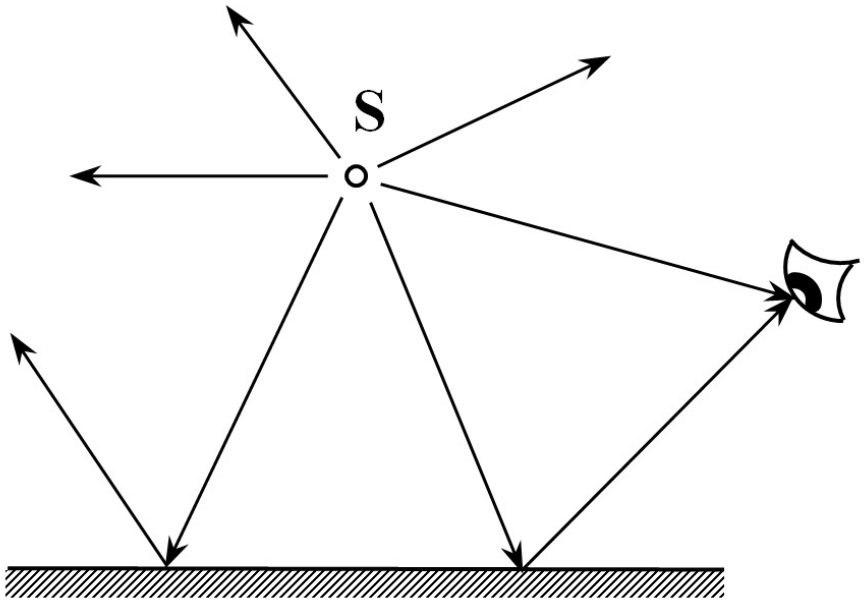

FIG. A1 – Photons emitted by light source S.

The number of photons emitted by a typical light source per second is unimaginably large (think of the number ten followed by 30 to 40 zeroes), and so we express this quantity in *LUMENS*, where one lumen is approximately the number of photons emitted per second by a wax candle[1]. A typical light source will emit tens of thousands of lumens.

A.3. Measuring Light

Photons emitted by light sources travel outwards in random directions. When these photons encounter a surface, they *ILLUMINATE* the surface (FIG. A2). From the perspective of the surface, it does not matter where the light comes from; it can be a single light source, multiple sources, or even the entire sky.

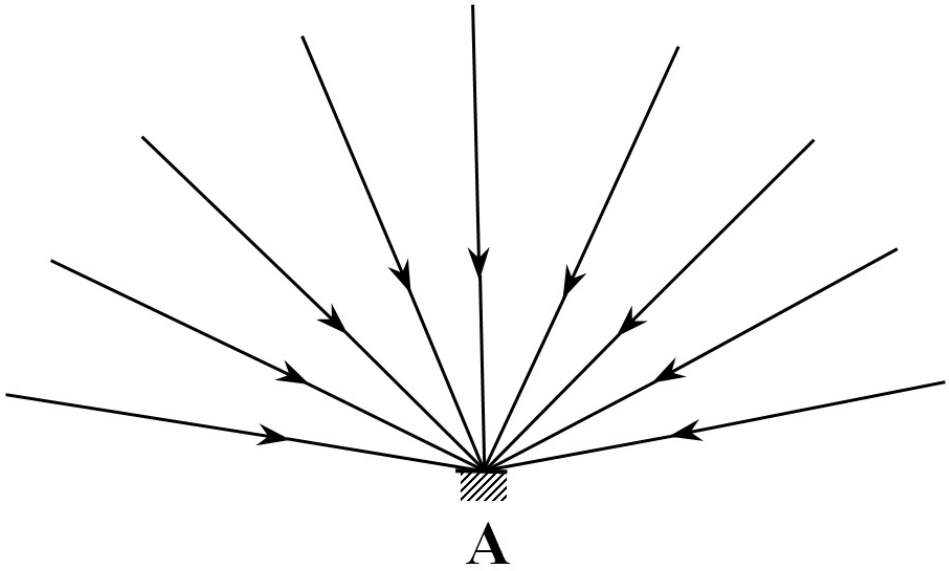

FIG. A2 – Light illuminating a surface A.

We can use a device called a *PHOTOMETER* to measure the number of photons arriving at (incident upon) the surface per second. Of course, this number will depend on the surface area of the photometer's' sensor, and so we express the *ILLUMINANCE* of the surface in terms of lumens per square meter, or *LUX*. (Lumens per square foot are referred to as a *FOOT-CANDLE* — please do not ask why.)

Note that the illuminated surface can be real or imaginary. We can, for example, imagine a "surface" positioned one meter above a physical surface, such as a playing field. The light will of course pass through this imaginary surface, but we can still measure its illuminance with a photometer (which is also called an "illuminance meter" by lighting designers or an "incident light meter" by photographers).

Illuminance is one of the two fundamental units of measurement for lighting designers. While we can measure illuminance with a photometer, we cannot see illuminance. For this, we need another fundamental unit of measurement.

Imagine looking at a computer display. The display consists of an array of a million or so pixels. We see each pixel because some of the photons it is emitting intersect our eye. We can therefore think of these photons as a ray of light, where all of the photons are traveling in the same direction. The more photons per second there are in the ray, the brighter the pixel appears to our eye. This is the *LUMINANCE* of the ray, sometimes referred to as "photometric brightness."

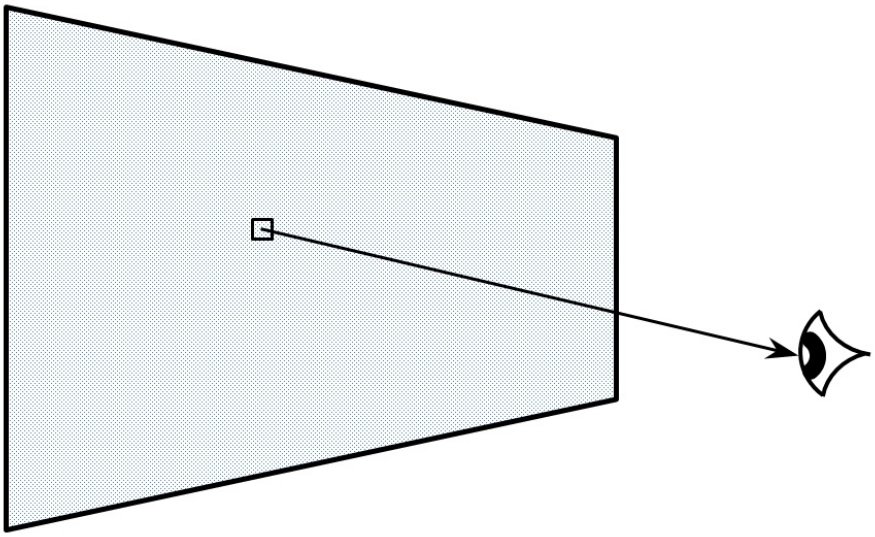

FIG. A3 – Light ray from a computer display pixel as seen by observer.

Textbooks on lighting design typically define luminance as the property of a real or imaginary surface, which leads to the very confusing unit of measurement, "lumens per square meter per steradian," or lm/m^2-sr. It is much easier, however (and just as accurate), to think of luminance as a property of the light ray itself. (The light we see coming from the blue sky, for example, has luminance, but it does not have a real or imaginary surface.)

We can easily measure the luminance of a ray by using a telescope to focus a narrow beam of light onto a photometer sensor (FIG. A4). This is a *LUMINANCE METER*; it measures what we see.

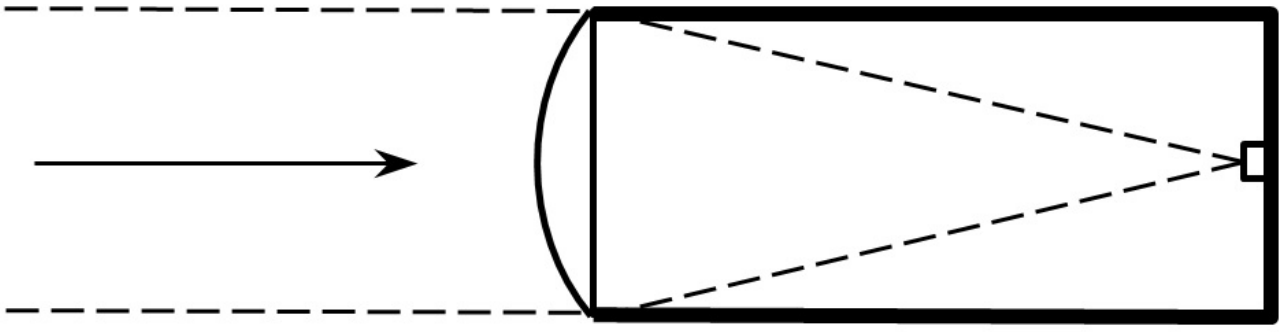

FIG. A4 – Luminance meter.

[1] A century ago, national standards for measuring light relied on precisely specified wax candles made from spermaceti (whale oil).

HORTICULTURAL INFORMATION

PHYTOCHROME AND PSS

Ian Ashdown, P. Eng., FIES, Senior Scientist, SunTracker Technologies Ltd. Published: 2016/12/09

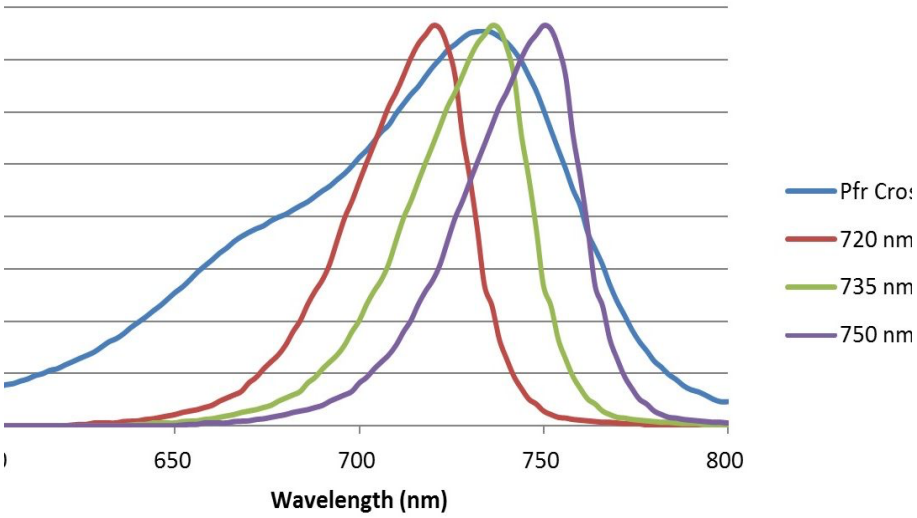

Horticultural lighting is currently one of the fastest-expanding markets in commercial lighting, with projected revenues of several billion dollars in less than a decade. From the perspective of a professional lighting designer, the market opportunities are enticing. Whether it is lighting for greenhouses or vertical farms and plant factories, the basic principles of lighting design remain the same.

FIG. 1 – Horticultural lighting in greenhouses. (Source: Colorado State University).

There are, however, design metrics that will be unfamiliar to most lighting designers. One of these — the subject of this article — has the rather unwieldy name of *PHYTOCHROME PHOTOSTATIONARY STATE* (PSS). While rarely discussed outside of horticultural research publications, it represents an important concept for horticulturists, and particularly floriculturists.

To understand this metric, it is necessary to review some aspects of plant biology.

Photomorphogenesis

The development of plants, from seed to flowering, is very much dependent on the electromagnetic radiation they are exposed to. This developmental process, called photomorphogenesis, is completely separate from the process of photosynthesis. It relies on various photopigments, including phytochromes, cryptochromes, phototropins, and UVR8, to sense and respond to radiation ranging from ultraviolet to near-infrared.

Our interest is in the photopigment family of phytochromes, which are mostly sensitive to red and far-red visible radiation. They mediate the germination of seeds (photoblasty), the growth of stems and leaves toward visible light (etiolation), the time of flowering based on the length of day and night (photoperiodism), the synthesis of chlorophyll for photosynthesis, and more (e.g., Smith 2000). While there are six known members of the phytochrome family, it is convenient to refer to them generically and collectively as “phytochrome.”

Phytochrome exists in two states, or *ISOFORMS*. In its ground state (identified as P_R), phytochrome strongly absorbs red light, and so appears turquoise-blue in concentrated solution *IN VITRO* (Figure 2). When it absorbs a red photon, however, it changes its physical shape to form its physiologically active state P_{FR}. In doing so, its peak spectral absorptance shifts towards the far-red, with a concentrated solution of phytochrome appearing more greenish in color.

When phytochrome is in its P_{FR} state, it may absorb a far-red photon and change once again into its P_R state. This bistable behavior makes phytochrome an ideal biochemical switch, with the P_{FR} isoform serving as the ìsignalingî state to the plant. As one example of this biological function, red light typically penetrates several centimeters into loose soil (e.g., Borthwick et al. 1952, Botto et al. 1996). As the sun rises higher each day in the spring, an increasing amount of red light reaches the seeds, until a sufficient concentration of phytochrome switches from its P_R isoform to its P_{FR} isoform. This signals the cellular mechanisms of the seed that it is time to sprout. If, on the other hand, the seed is buried too deeply, it will never sprout and will eventually die.

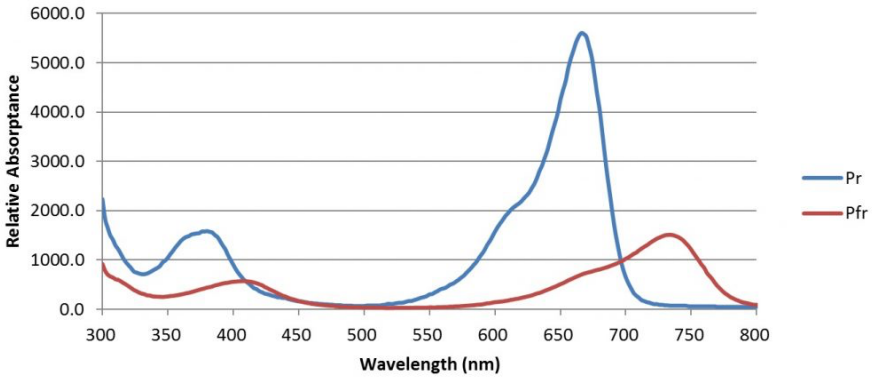

FIG. 2 – Phytochrome spectral absorptance. (Source: Sager et al. 1988).

Photoperiodism

The existence of phytochrome was first suspected nearly a century ago, when Garner and Allard (1920) studied the effects of day length on flowering plants. They observed that tobacco plants could be made to flower in summer by reducing the hours of daylight with artificial darkening, and that they could also be made to remain in a vegetative state during the winter by providing supplemental electric light. They called this effect photoperiodism.

Some plant species flower only when exposed to short periods of light (such as poinsettias — Islam et al. 2014), and so are called *SHORT-DAY* plants, while others flower only after to exposure to long periods of light (such as spinach and radishes), and are called *LONG-DAY PLANTS*. In some *DAY-NEUTRAL* plants (such as tomatoes), flowering is not regulated by photoperiod.

The reason for these reactions in both short-day and long-day plants is the response of phytochrome to red and far-red light. With short-day plants, exposure to a brief period of light during the night inhibits flowering, while the same exposure with long-day plants promotes flowering. Floriculturists can therefore use supplemental electric lighting to delay or advance the flowering of plants to meet market needs.

The traditional techniques for photoperiodic control include (Boyle 1992):

- Increasing the day length — While high-pressure sodium (HPS) lamps have traditionally been used for supplemental greenhouse lighting, incandescent lamps have the advantage of being rich in red and far-red radiation. Compact and linear fluorescent lamps have also been used, but their relative lack of red and far-red radiation makes them ineffective for phytochrome response manipulation.
- Night interruption — The phytochrome response to red and far-red radiation does not require continual exposure. Consequently, the flowering period can be influenced with only a few hours of electric lighting during the night. This has the advantage of being more energy-efficient.
- Cyclic (intermittent) lighting — If incandescent rather than HPS lamps are used, it may be sufficient to pulse the lighting with a short duty factor, such as one minute every half hour. (The optimal duty factor will depend on the irradiance at the plant canopy.)
- Shortening the day length — The plants are covered with an opaque material to reduce the irradiance, preferably to the equivalent of less than 20 lux of visible light. Typical materials are black sateen cloth, woven polyolefin sheeting, and black polyethylene films.

The problem with these techniques is that they are mostly trial-and-error with different plant species and greenhouse operation conditions. The goal is to manipulate the plant growth and development through the phytochrome response, but there is no practical means of quantitatively predicting the impact of these techniques.

Solid State Lighting

The introduction of solid state lighting to the horticultural industry has been nothing short of revolutionary. In addition to the energy savings afforded by the use of blue and red LEDs whose spectral power distributions (SPDs) are optimal for photosynthesis (Figure 1), the recent commercial availability of high-flux red and far-red LEDs from manufacturers such as Lumileds, Osram, and Cree means that horticulturists and floriculturists now have the ability to precisely tune the light source SPDs for optimal photoperiod control on a per-species basis.

While the LED manufacturers' product names vary, the products of interest have peak spectral outputs at 660 nm and 730 nm, corresponding to the peak spectral absorptances of phytochrome isoforms P_R and P_{FR}, respectively (Figure 2). The key here is that the ratio of red to far-red light can be easily set or varied on a daily basis as required for photoperiodic control. Along with blue LEDs, this ability to precisely control the light source SPD leads to the promise of plant "light recipes," where the SPD and other environmental factors can be chosen on a per-species basis, and possibly varied over the life cycle of the plant growth and development.

The problem, of course, is that in order to control something, you need to measure it. For professional lighting designers, you also need the ability to specify it.

PSS Metric

The *PHYTOCHROME PHOTOSTATIONARY STATE* (PSS) metric was introduced some two decades ago (Sager et al. 1998). It has been mostly of academic interest with HPS and incandescent lighting, but the introduction of LEDs for horticultural lighting has suddenly brought this metric to the forefront as a useful design tool.

The metric is conceptually simple: it is the ratio of the concentration of the P_R isoform of phytochrome to the total concentration of both isoforms:

$$PSS = \frac{P_r}{P_r + P_{fr}}$$

under constant irradiation by a light source. (The maximum value is less than unity because of the spectral overlap between the two isoforms.)

By itself, this seems of little to no interest to lighting designers — how do you measure the relative concentrations of the phytochrome isoforms in a plant? (It took nearly forty years from the time of Garner and Allard (1920) just to isolate phytochrome in the laboratory — Butler et al. 1959.)
What Sager and his fellow researchers did was to note that each phytochrome molecule could be conceptually modeled as an opaque sphere that fully absorbs any incident radiation. If you measure the spectral absorptance of the molecule in solution and know the concentration, you can calculate the equivalent photochemical cross-section of the molecule for each wavelength. (As an aside, LED manufacturers use exactly the same approach when modeling the optical characteristics of LED phosphors embedded in an epoxy or silicone matrix.)

With this, Sager et al. measured the spectral absorptance of the P_R and P_{FR} isoforms (reproduced in Figure 2) and expressed the results as phytochrome photochemical cross-sections, measured in square meters per mole (i.e., 6.022 x 10^{23} molecules), represented as σ_R and σ_{FR}, respectively. Equation (1) then becomes:

$$PSS = \frac{\sum_{300}^{800} N(\lambda)\sigma_r(\lambda)}{\left(\sum_{300}^{800} N(\lambda)\sigma_r(\lambda) + \sum_{300}^{800} N(\lambda)\sigma_{fr}(\lambda)\right)}$$

where $N(\Lambda)$ is the measured spectral photon flux for wavelength Λ over the range of 300 nm to 800nm.

For photometric test laboratories characterizing horticultural luminaires, all that needs to be done is to measure the luminaire's relative spectral power distribution. Calculating the PSS metric using the photochemical cross-section data from Sager et al. (1988) in accordance with Equation 2 is then a simple spreadsheet exercise.

For professional lighting designers, it is even simpler: the PSS metric is a direct indication of the ability of the horticultural luminaire to manipulate the phytochrome isoforms. While this will also depend, of course, on the absolute irradiance at the plant canopy, the PSS metric reduces the spectral power distributions of the red and far-red LEDs to a single number that can be specified.

LED Color Binning

We are not done yet! Professional lighting designers are all too familiar with the issue of precision in lighting design metrics. For example, lamp and luminaire manufacturers typically report the CIE General Colour Rendering Index (CRI) using two digits, such as CRI = 92. If you refer to the history of the CRI metricís development, however, you will learn that the intended precision of this metric is five units (van Trigt, 1999). In other words, the difference between CRI = 90 and CRI = 92 is visually imperceptible and so meaningless in terms of practical application.

The same question must be asked of the PSS metric. Is, for example, PSS = 0.39 quantitatively different from PSS = 0.38? Perhaps surprisingly, this is not a question for horticultural researchers. Rather, it is a question for lighting researchers and the lighting industry.

The underlying problem is a familiar one: LED color binning. Taking Lumiledís LUXEON SunPlus 20 series of horticultural LEDs as typical examples, we have:

Product Name	Minimum Peak Wavelength	Maximum Peak Wavelength
Deep Red	655	670
Far Red	720	750

Table 1 – LUXEON SunPlus 20 peak wavelength binning. (Source: Lumileds 2016).

The Lumileds product datasheet provides typical spectral power distributions for these two products with typical peak wavelengths, which can be digitized and shifted to represent the minimum, typical, and maximum peak wavelength SPDs, as shown in Figures 3 and 4. These figures also display the red P_R and far-red P_{FR} phytochrome spectral photochemical cross-sections (i.e., their spectral absorptances), with the SPDs normalized to the peak cross-sections for display purposes only.

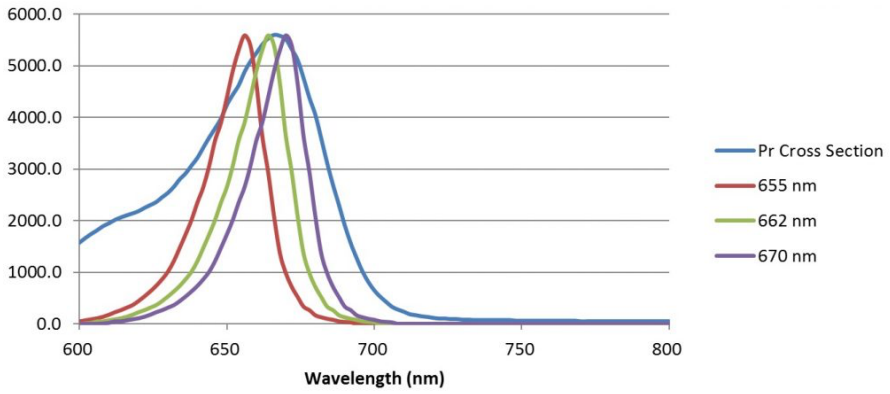

FIG. 3 – Lumileds SunPlus 20 Deep Red.

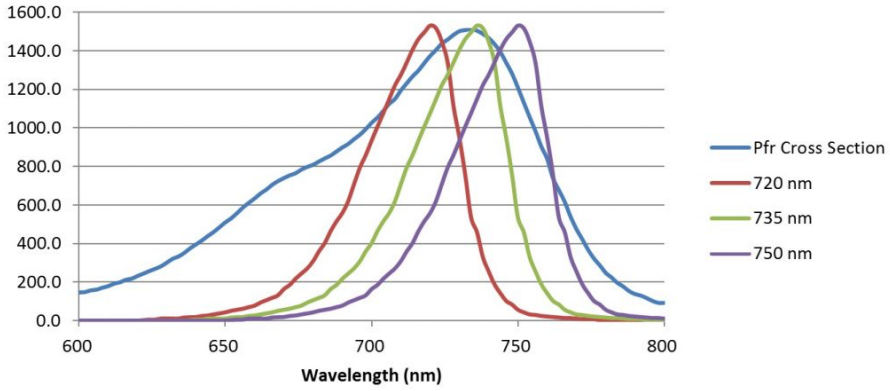

FIG. 4 – Lumileds SunPlus 20 Far Red.

From this information, and assuming that the peak spectral photon intensities of the red and far-red LEDs are the same, the phytochrome photostationary state (PSS) metric values can be calculated as follows:

	Minimum	Typical	Maximum
PSS	0.3563	0.3797	0.4036

Table 2 – Example PSS values range (2-nm resolution)

In other words, the PSS value may vary by approximately ±6 percent for a given luminaire manufacturer's product. This is useful information for lighting designers when specifying or qualifying horticultural luminaire products, similar to the meaningful precision of the CRI metric.

There is one further question to address. Sager et al. (1988) reported the photochemical cross-section values σ_R and σ_{FR} at 2-nanometer intervals. This is useful from an academic perspective, but perhaps not so much from that of a photometric testing laboratory. Unless the laboratory performs the LED spectral power distribution measurements in-house, it is likely that the SPDs will be available in 5 nm increments only. While this data can be interpolated at 2-nm intervals for the purposes of calculating the PSS metric in accordance with Equation 2, will the difference in calculated results be significant? To answer this question, the σ_R and σ_{FR} values published in Sager et al. (1988) were interpolated at 5-nm intervals using a cubic spline approximation, and Table 2 was recalculated using 5-nm resolution for the LED spectral power distributions:

	Minimum	Typical	Maximum
PSS	0.3639	0.3639	0.3639

Table 3 – Example PSS values range (5-nm resolution)

In this situation, the PSS value may vary by approximately ±5 percent for a given luminaire manufacturer's product. More significantly, the PSS value for 5-nm resolution was only two percent higher than the PSS value with 2-nm resolution.

These results will of course vary for different typical PSS values, but likely not significantly.

As rules of thumb, therefore:

- Differences in PSS values of less than ±5 percent are likely not significant.
- It likely does not matter whether the PSS values are calculated using 2-nm or 5-nm resolution.

The qualifier "likely" recognizes that, while the PSS metric is some two decades old, greenhouse operators have yet to make use of it as a production tool. Future experience may indicate that these rules of thumb are too lax. In the meantime, however, the above analysis provides some guidance for both lighting designers and horticulturists.

Conclusion

Horticultural lighting presents interesting opportunities for professional lighting designers. It is a rapidly developing field where the use of blue and red LEDs for optimal photosynthesis is only the beginning. Solid state lighting has energized horticultural research into plant responses to light sources with different spectral power distributions, and there will surely be discoveries that improve our understanding of both photosynthesis and photomorphogenesis, as well as improvements in horticultural lighting design.

In the meantime, the phytochrome photostationary state (PSS) metric is an example of existing knowledge that will likely prove useful in designing and specifying horticultural lighting systems.

References

Borthwick, H.A., S. B. Hendricks, M. W. Parker, E. H. Toole, and V. K. Toole. 1952. "A Reversible Photoreaction Controlling Seed Germination," Proceedings of the National Academy of Science 38:662-666.

Botto, J. F., R. A. S·nchez, G. C. Whitelam, and J. J. Casal. 1996. "Phytochrome A Mediates the Promotion of Seed Germination by Very Low Fluences of Light and Canopy Shade Light in Arabidopsis," Plant Physiology 110:439-444.

Butler, W. L., K. H. Norris, H. W. Siegelman, and S. B. Hendricks. 1959. "Detection, Assay, and Preliminary Purification of the Pigment Controlling Photoresponsive Development of Plants," Proc. National Academy of Sciences 45:1703-1708.

Boyle, T. 1992. "Photoperiod Control Systems for Greenhouse Crops," Floral Notes 4(6):2-4. (See also Photoperiod Control Systems for Greenhouse Crops.)

Garner, W. W., and H. A. Allard. 1920. "Effect of the Relative Length of Day and Night and Other Factors of the Environment on Growth and Reproduction in Plants," Journal of Agricultural Research 18:553-606.

Islam, M. A., D. Tarkowská, J. L. Clarke, D.-R. Blystad, H. R. Gislerød, S. Torre, and J. E. Olsen. 2014. "Impact of End-of-day Red and Far-red Light on Plant Morphology and Hormone Physiology of Poinsettia," Scientia Horticulturae 174:77-86.

Lumileds. 2016. DS171 LUXEON SunPlus Series for Horticulture, Lumileds Product Datasheet 20160908.

Sager, J. C., W. O. Smith, J. L. Edwards, and K. L. Cyr. 1988. "Photosynthetic Efficiency and Phytochrome Equilibria Determination Using Spectral Data," Trans. ASAE 31(5):1882-1889.

Smith, H. 2000. "Phytochromes and Light Signal Perception by Plants — An Emerging Synthesis," Nature 407:585-591.

van Trigt, C. 1999. "Color Rendering, A Reassessment." *COLOR RESEARCH & APPLICATION* 24(3):197-206.

ENTERTAINMENT INFORMATION

CONTROLLING MULTICOLOR LED LUMINAIRES

Ian Ashdown, P. Eng., FIES, Senior Scientist, SunTracker Technologies Ltd. Published: 2016/06/11

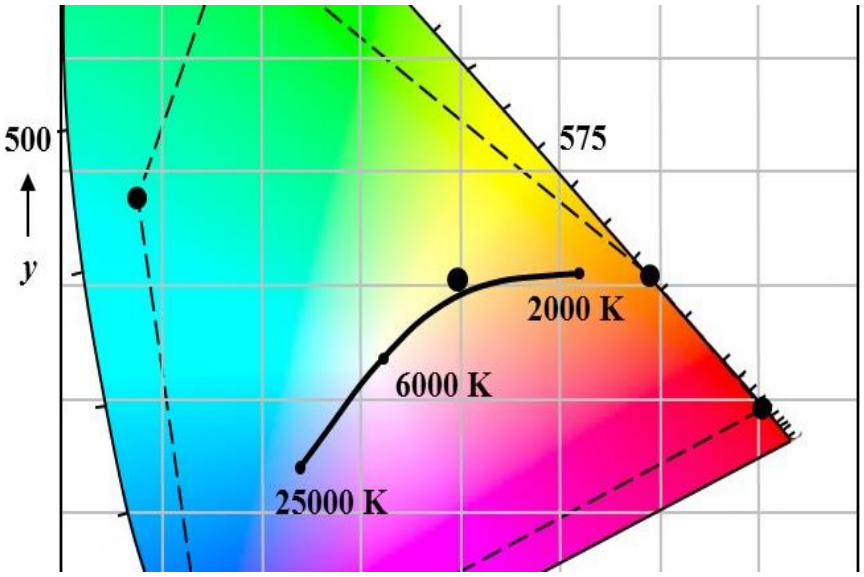

SAN JOSE, CA, USA: MARCH 31, 2016.

LED ENGIN, INC. ANNOUNCES THE WORLD'S FIRST 7-COLOR, HIGH POWER LED TO BE PRODUCED ON A SINGLE EMITTER. THE COMPACT LZ704MU00 EMITTER ENABLES THE DESIGN OF STAGE OR ARCHITECTURAL LIGHTING THAT PRODUCES SOPHISTICATED EFFECTS OVER THE FULL COLOR SPECTRUM. ITS RGBW DIE ARE COMPLEMENTED BY PHOSPHOR-CONVERTED (PC) AMBER, CYAN AND VIOLET TO PROVIDE RICHER, WIDE-RANGING COLOR EFFECTS. PC AMBER DELIVERS THE SAME SATURATION AS REGULAR AMBER BUT WITH 5 TIMES THE FLUX AT TEMPERATURE, CYAN FILLS THE SPECTRUM GAP BETWEEN BLUE AND GREEN, AND VIOLET ENABLES BLACK OR CRISP WHITE LIGHTING EFFECTS. TYPICAL STAGE AND STUDIO APPLICATIONS INCLUDE MOVING HEADS WITH ZOOM OPTICS AND ROUND WASH LIGHTS. IN ARCHITECTURAL LIGHTING, THE EMITTERS ENHANCE THE PERFORMANCE OF EVERYTHING FROM STATIC LIGHTS TO LINEAR WASH LIGHTS…

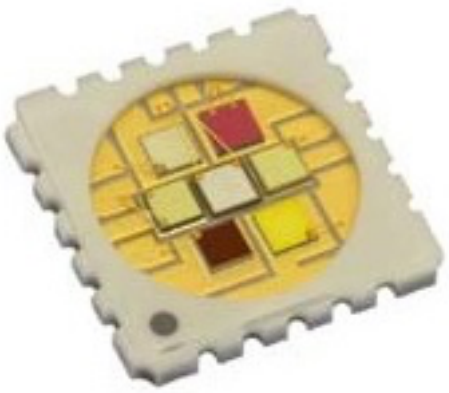

FIG. 1 – LED Engin seven-color LED package (www.ledengin.com).

The reason for this lengthy quote from *LED ENGIN*'s press release is that it succinctly introduces the background to this blog article. Multicolor LED luminaires are nothing new – the theatrical lighting industry saw them introduced nearly a decade ago, with products such as the *ETC SELADOR DESIRE* series of seven-color LED luminaires (FIG. 2).

FIG. 2 – ETC Selador Desire seven-color LED luminaire (www.etcconnect.com).

What is new and significant about the *LED ENGIN* product announcement is that having seven different color LED die in a single package enables manufacturers to design potentially more compact luminaires that do not exhibit multicolor shadows at close range.

What is equally significant, however, is that there is a problem with multicolor LED luminaires, a serious problem that has been basically overlooked for the past decade. This blog article offers a potential solution.

A Matter of Control

To understand the problem, first consider color-changing LED modules with red, green, and blue (RGB) LEDs. Generating a specific color is a simple matter of choosing the appropriate ratios of the red, green, and blue LED intensities. For example, if we want to generated 4150K white light, we might choose the intensity ratios shown in FIG. 3.

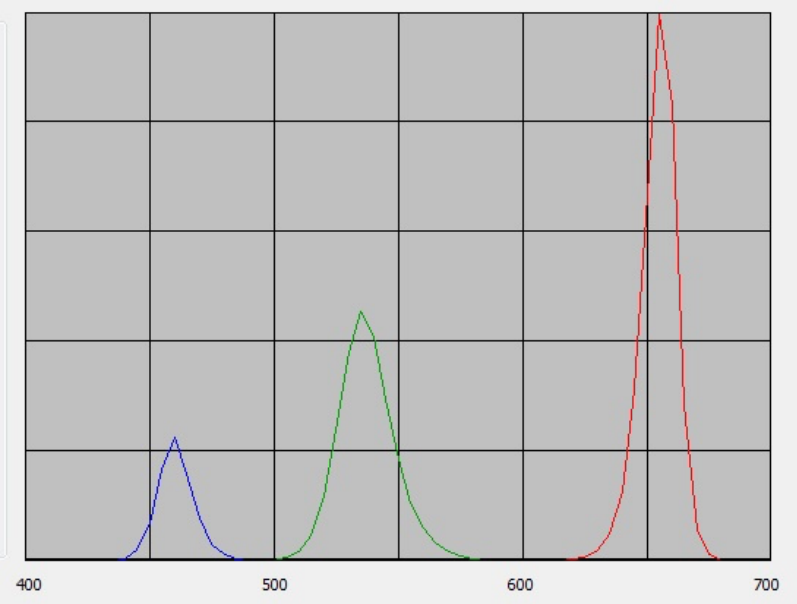

FIG. 3 – Three-color 4150K white light source spectral power distribution.

As any theatrical lighting designer will quickly point out, however, there are two problems with RGB LED modules and luminaires. First, their color gamuts are fairly limited. In particular, they are typically unable to produce saturated blue, violet, and cyan colors (e.g., FIG. 4).

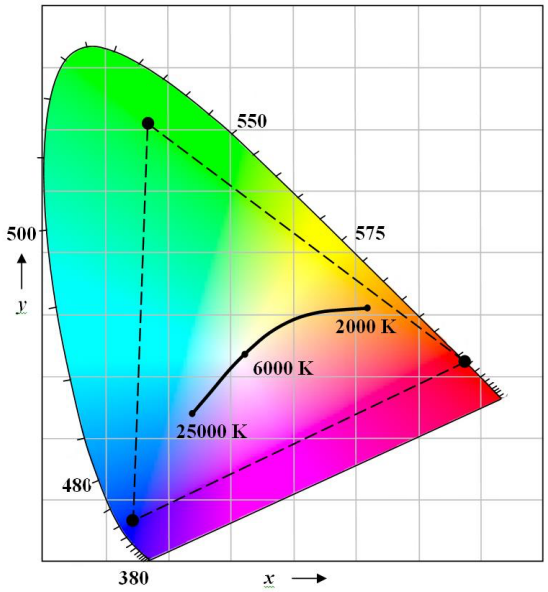

FIG. 4 – Typical RGB LED module color gamut.

Second, the lack of spectral radiant flux between approximately 550 nm and 600 nm, generally perceived as yellow light, results in yellow objects illuminated by RGB light sources appearing dull and lifeless in comparison to an equivalent white light source. Given a choice, most theatrical lighting designers would probably choose a conventional quartz-halogen luminaire (with a color temperature of 3200 Kelvin) and a Rosco 202 Half CT Blue polyester color filter to raise its color temperature to approximately 4150K. For professional stage lighting, color quality is paramount.

The disadvantage, of course, is that even with motorized color filter wheels, quartz halogen luminaires offer limited dynamic color opportunities. If the designer needs to change colors during or between scenes, multiple luminaires are generally required. This is why multicolor LED luminaires are so attractive – with six or seven colors, they provide larger color gamuts (e.g., FIG. 5), smooth transitions between colors are possible, and they do not suffer from the color rendering issues of RGB luminaires.

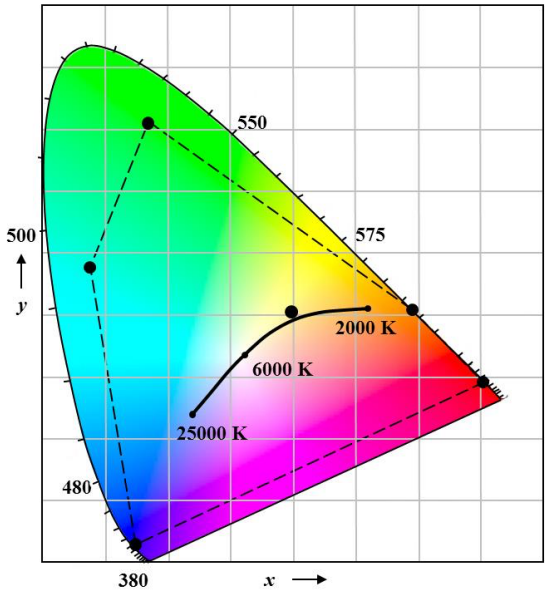

FIG. 5 – Six-color LED module color gamut.

The problem is that there are now six or seven LED intensities to control if you need to generate a specified color. Unlike RGB LED modules, there are basically an infinite number of LED intensity combinations to choose from.

As an example, suppose we are given a six-color LED module with the following colors:

- Blue (440 nm)
- Cyan (495 nm)
- Green (525 nm)
- Amber (595 nm)
- Red (630 nm)
- White (3000K)

We need to generate 4150K white light, for which we find through laborious trial-and-error with a colorimeter are the two solutions shown in Figures 6A and 6B – two very different solutions with radically different spectral power distributions (SPDs), and with relative LED intensity ratios shown in Table 1. (The luminous efficacies and quantities of LEDs per color vary; the intensities are in relation to their full power settings.)

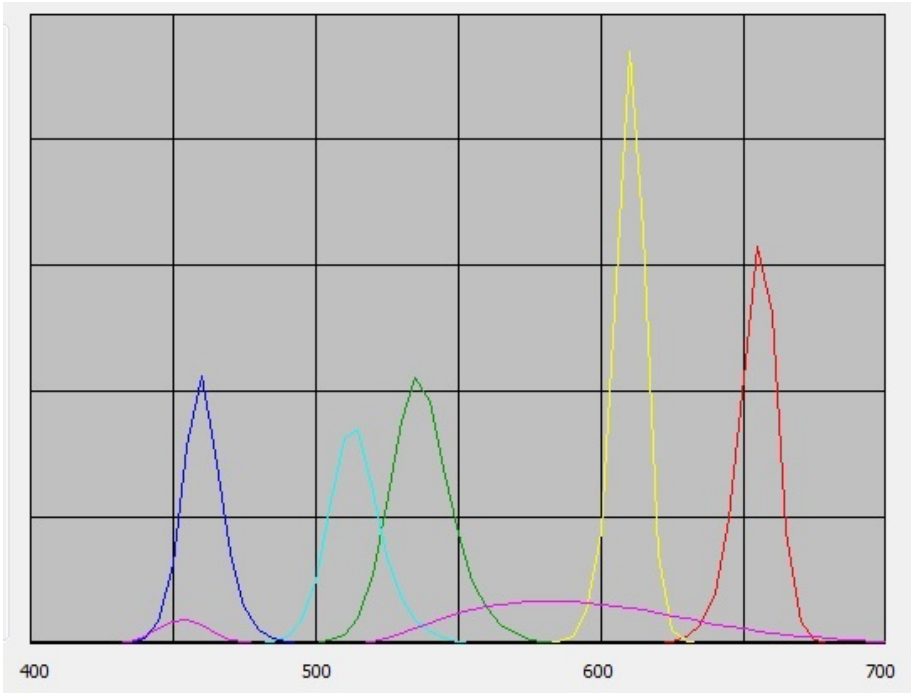

FIG. 6A – Six-color 4150K white light SPD (first example).

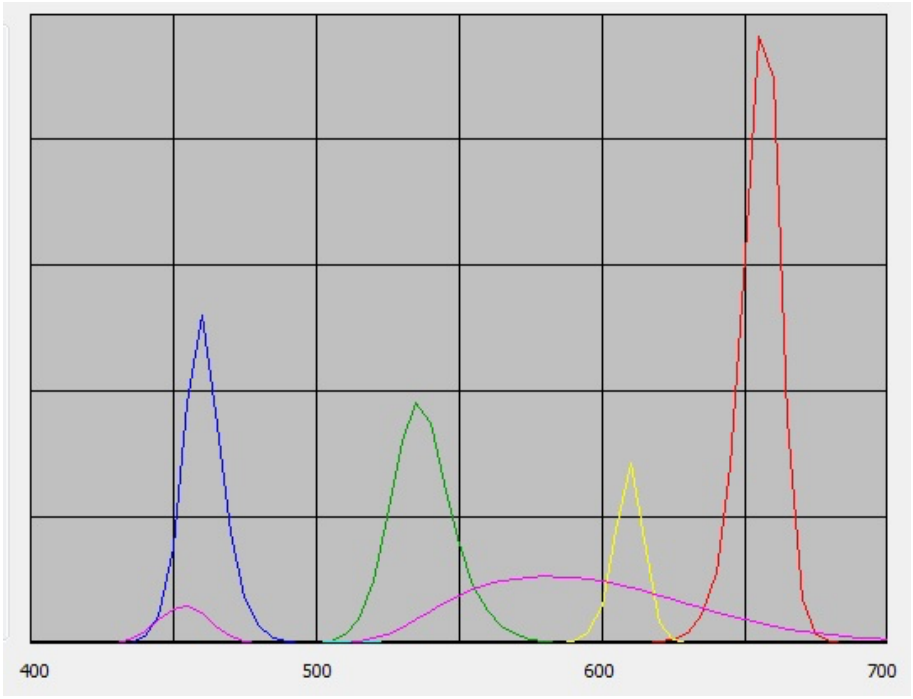

FIG. 6B – Six-color 4150K white light SPD (second example).

Color	Example 1	Example 2
Red	1.00	1.00
Amber	1.00	0.18
Green	0.85	0.51
Cyan	0.18	0.00
Blue	0.20	0.10
White	1.00	1.00
Intensirt	2712	1471
CRI Ra	62	27

Table 1 – Multicolor LED relative intensities comparison

The important point here is that while both solutions may look the same visually, the second example generates only 54 percent as much luminous flux (i.e., lumens) as the first example. (This makes sense, of course, as the human eye is more sensitive to amber light than it is to red light.)

Another point is that while the first example may generate more luminous flux, the second example has much better color rendering properties due to the greater amount of amber light. (A CRI Ra value of 62 versus 27.)

This is the problem with multicolor LED luminaires – how do you choose the "best" solution from an infinite number of relative intensity ratios for a given color? It depends, of course, on whether "best" means maximum luminous intensity or color rendering properties, such as the CIE Ra and R9 color rendering metrics for white light. (There are no established color rendering metrics for chromatic illumination, but they conceivably could be developed.)

The situation is exacerbated if you need to transition between two colors while maintaining constant intensity. Multicolor LED luminaires are clearly capable of doing this, but you need to determine the best solution for all the intermediate colors, preferably fifty or more times a second during the transition to prevent visible flickering.

Manufacturers of multicolor LED luminaires have overlooked this problem from the beginning. The *ETC SELADOR DESIRE* products, for example, present the user with one DMX512 intensity control channel per color, plus a master intensity control channel for all colors. It is a control solution that offers no solution.

To be fair, the manufacturers cannot be faulted for taking this approach. In mathematical terms, the choice of relative intensity ratios is an "overdetermined" problem, where the number of variables (e.g., the number of LED colors) exceeds the number of outputs (e.g., the red, green, and blue primary colors that the human eye is sensitive to).

This is not to say that the problem is unsolvable – it is. If a million monkeys with typewriters will eventually reproduce all the works of Shakespeare, we can take the same approach (albeit with fewer monkeys) to determining the best solution for a given color.

The “we” in this situation are the luminaire manufacturers and designers. It is basically a product design problem that does not involve the end user. What follows is a reasonably detailed outline of the design of an effective user interface for multicolor LED luminaires.

Solving the Problem

We begin with the acknowledgement that we need to know something about the optical, electrical, and thermal properties of the different color LEDs in order to predict how much light they will generate under various operating conditions. Specifically, we need to know for each color LED:

- Spectral power distribution
- Luminous efficacy (lumens per watt)
- Maximum current (at full intensity)
- Forward voltage
- Dynamic resistance
- LED package thermal resistance
- LED substrate temperature

and also the desired color, or “target chromaticity,” expressed in CIE 1931 *XY* chromaticity coordinates. (Note that the spectral power distribution is dependent on the LED junction temperature.)

A proof-of-concept program called *SSL DESIGNER™* was developed for this approach, with a screenshot of the above system parameters shown in Figure 7.

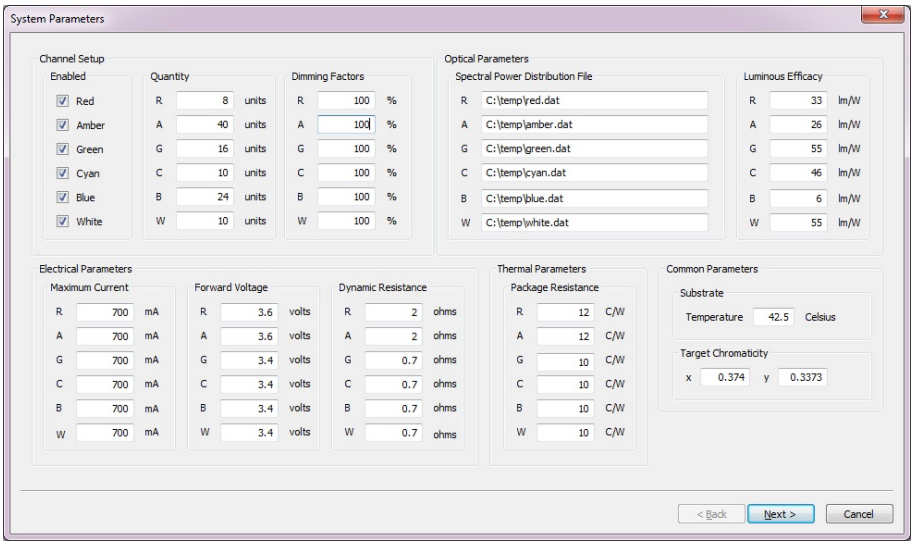

FIG. 7 – SSL Designer system parameters.

Given this information, it is possible to calculate the absolute spectral power distribution for each color LED. These SPDs can then be scaled by the relative intensity ratios (shown in FIG. 8) as channel PWM duty cycles), following which they are summed and the luminous intensity calculated. (With a bit more work, color rendering metrics such as CIE Ra and R9 for white light applications can also be calculated.)

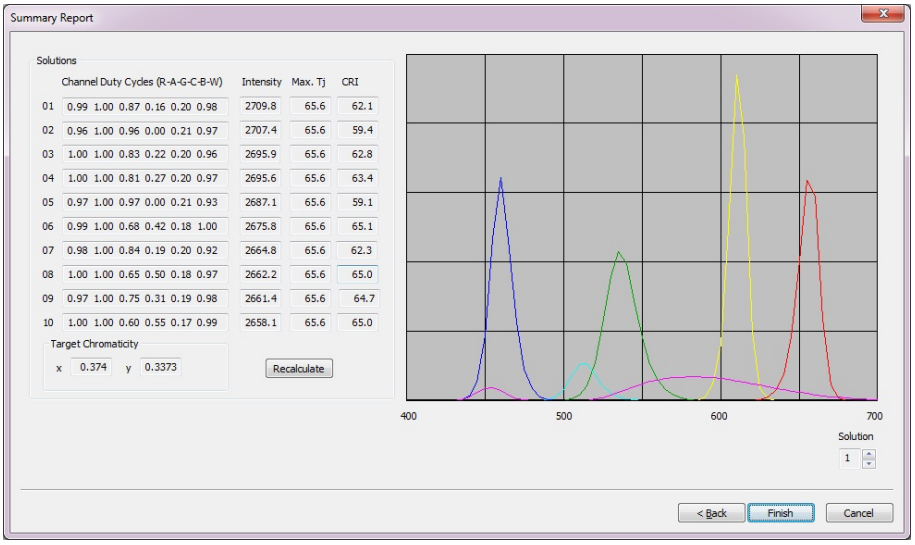

FIG. 8 – Ten best relative intensity ratio solutions for specified color.

There are ten relative intensity ratio solutions shown in FIG. 8, but these are the best (in the sense of maximum luminous intensity) of tens of thousands of randomly selected solutions that have been evaluated. Of course, it is highly unlikely that a random choice of relative intensity ratios will generate the desired target chromaticity, but some solutions will be closer than others. An evolutionary computation approach called a genetic algorithm is therefore used to intelligently and quickly select and refine those solutions that satisfy the target chromaticity criterion (and optionally one or more-color rendering metric criteria), and to order them accordingly as the best solutions. Again, in mathematical terms, the genetic algorithm "converges" to the best solutions.

Not shown in Figure 8 is the ability to calculate the best solutions for hundreds of different target chromaticities, which are then stored in memory. When the user later specifies a desired color, the program finds the best solution for the nearest matching color, then uses this to "seed" the initial randomly selected solutions. The genetic algorithm can then converge much more quickly to the best solution.

An RGB Solution

In practice, the user needs to specify both the desired color and intensity. This can be done using CIE *XYY* values, where *XY* represent the CIE 1931 chromaticity coordinates (shown as the horizontal and vertical axes in FIG. 5), and *Y* represents the intensity (expressed as a percentage of maximum intensity). This approach is, however, not as intuitive as the RGB settings most lighting designers are familiar with.

Fortunately, there is a simple solution. Referring to the six-color LED module color gamut shown in Figure 5, we can completely enclose the six-sided color gamut in a triangle defined by the *XY* chromaticities of virtual red, green, and blue LEDs (FIG. 9). It does not matter that the red LED chromaticity lies outside the horseshoe-shaped spectral locus and so represents a physically impossible color. What does matter is that the RGB values can be used to represent any color (and intensity) within the six-color LED module color gamut.

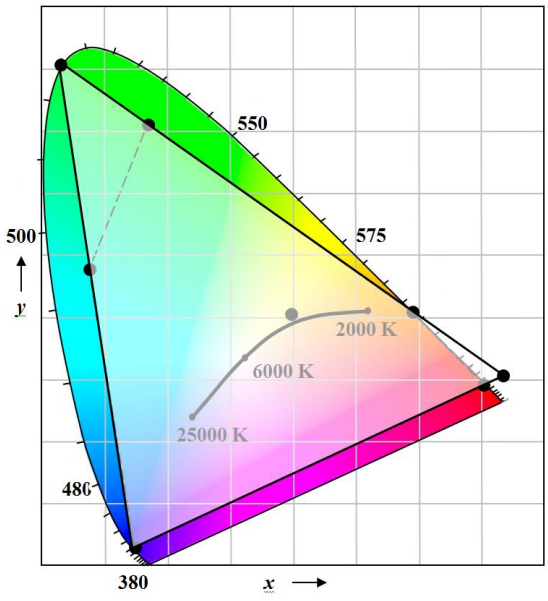

FIG. 9 – Virtual RGB LED module color gamut.

The mathematics needed to transform the RGB values to CIE *XYY* values are straightforward to calculate – a task that is performed by the luminaire's microcontroller. From the user's perspective, all that is needed are three DMX512 channels to control the luminaire, which will appear to behave as an RGB LED luminaire with enhanced color rendering capabilities.

A decade ago, this approach would have been impractical due to the computing power requirements. Today, however, it is both practical and economical to embed a microcontroller in the luminaire that will perform the necessary calculations in real time (i.e., milliseconds).

Public Service

The *SSL DESIGNER* software developed to demonstrate this novel approach is a proof-of-concept program that simulates a multicolor LED luminaire on a desktop computer. Following standard industry practice, it would make sense to apply for a patent on the invention and license the technology to theatrical luminaire manufacturers.

Most countries have differing intellectual property laws, but they all agree that if an invention is publicly disclosed prior to filing a patent application, it is ineligible for patent protection. This blog article therefore represents an intentional and deliberate public disclosure of the invention. Specifically, this invention has been released into the public domain. No patent application has been

filed, and so lighting manufacturers and designers are both free and encouraged to implement the above royalty-free approach in their multicolor LED luminaire products.

In the spirit of published patents, there are numerous implementation details that have been glossed over in this article. However, the details that have been presented are “sufficient for one skilled in the art” to implement the invention “without undue experimentation” (35 U.S.C. 112(a), www.uspto.gov). Anyone curious about the implementation details of *SSL DESIGNER* is welcome to contact the author with questions.

Multicolor LED luminaires have been commercially available for nearly ten years. It is time for the luminaire manufacturers and designers to make them truly useful.

DAYLIGHTING INFORMATION

CLIMATE-BASED DAYLIGHT MODELING

Ian Ashdown, P. Eng., FIES, Senior Scientist, SunTracker Technologies Ltd. Published: 2016/03/26

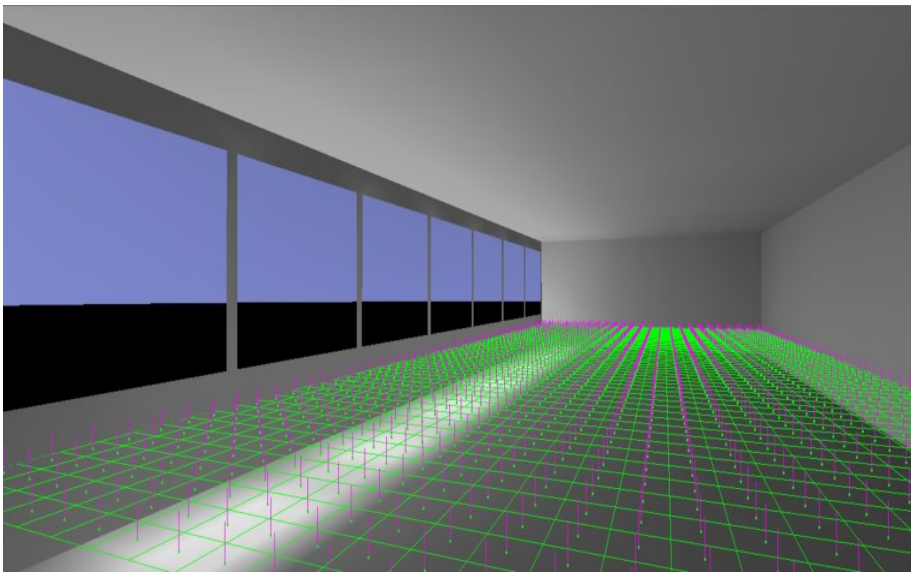

DAYLIGHT, n. The light of day.

Apart from having a wonderfully circular definition in most English-language dictionaries, daylight really is just another form of illumination. As such, most people would expect lighting designers to be able to simulate daylight with the same ease that we simulate electric lighting … but ah, I see you blushing.

We have for the past one hundred and fifty years relied on daylight factors to predict the distribution of daylight in architectural spaces. The daylight factor metric is exceedingly simple to calculate, but it is not very useful in understanding how daylight illuminates an interior space. All it really tells us (and our clients) is whether there will be sufficient daylight to read a newspaper indoors on an overcast day. We have, in other words, good reason to blush.

We know better, of course. Given the architectural plans of a building, including both its geographical coordinates and orientation, we know we can use historical weather data to determine the typical distribution of daylight within the building for every hour of every day of the year. We even have a name for this: *CLIMATE-BASED DAYLIGHT MODELING* (CBDM), an expression introduced a decade ago at a CIBSE lighting conference appropriately called “Engineering the Future” (Mardaljevic 2006).

With CBDM, we can calculate daylight metrics such as *SPATIAL DAYLIGHT AVAILABILITY* and *ANNUAL SUNLIGHT EXPOSURE* (IES 2012), *USEFUL DAYLIGHT ILLUMINANCE* (Nabil et al. 2006), *DAYLIGHT GLARE PROBABILITY* (Wienold et al. 2006), and more. The first two metrics are important in that they are necessary for earning all three LEED v4 daylighting credit points (USGBC 2013). As consultants to architectural firms, lighting design professionals have an obligation to provide these metrics. Glare

metrics take this one step further, offering the ability to identify potential design problems with large expanses of glazing.

Going further still, we can design and validate daylight harvesting systems for energy savings, and address building energy modeling issues involving solar insolation. Most important, we can work with architects during the conceptual design phase to take full advantage of what daylighting has to offer. From a lighting design perspective, CBDM expands the consulting services we can provide.
… and yet we persist in using daylight factors for our lighting design work.

The problem for most lighting designers is that the practice of climate-based daylight modeling is anything but simple. Until recently, the only software capable of performing CBDM calculations has been Lawrence Berkeley National Laboratory's *RADIANCE* … and here I must pause.

Radiance

RADIANCE is — there are no other words to describe it — an exceedingly powerful, and indeed wonderful, set of software tools for electric lighting and daylighting research. It is not a monolithic program, but rather a set of one hundred or so Unix programs that can be linked together using command-line scripts.

RADIANCE, however, is first and foremost a research tool. It is reasonable to assume that most architects and engineers will prefer not to learn Unix, with command-line scripts such as:

```
vwrays -fa -vf views/v2.vf -x 600 -y 600 | \
    rfluxmtx -n 8 'vwrays -vf views/v2.vf -x 600 -y 600 -d' \
    -fac -ab 6 -ad 1000 -lw 1e-3 - objects/LP_bottom.rad \
    materials_light.rad model.rad
```

Fortunately, there are a number of free and commercial architectural-engineering design applications that are available, and which provide graphical user interfaces to the *RADIANCE* toolset. Those that support climate-based daylight modeling include *DAYSIM* and *DIVA FOR RHINO* (www.daysim.ning.com).

This article is not, however, about *RADIANCE* and its derivatives; it is about climate-based daylight modeling. More particularly, it is about a unique radiosity-based approach to CBDM calculations that does not involve the *RADIANCE* daylight calculation engine. It is the culmination of over twelve years of research and development, beginning with the paper "Modeling Daylight for Interior Environments" (Ashdown 2004). The details are disclosed herein for those interested in understanding how it works.

Follow the Light

In order to fully understand the radiosity approach, it is necessary to follow the light from source to receiver. The source is the combination of direct sunlight and diffuse daylight; the receiver is a room or similar naturally illuminated space within a building.

Modeling direct sunlight is straightforward. The solar position in the sky can be readily calculated from the equations presented in Section 7.1.5, Solar Position, of the IESNA Lighting Handbook, Tenth Edition (IES 2011). The solar disk is only 0.5 degrees in apparent width, and so it can be reasonably modeled as an infinitely distant point source that produces a beam of light whose rays are parallel. Modeling diffuse daylight is more challenging. Some of the extraterrestrial radiation from the sun is scattered by the Earth's atmosphere, resulting in the hemispherical diffuse light source that is the sky. The sky *LUMINANCE* (colloquially, "brightness") spatial distribution varies with geographic location, site altitude, time of day, time of year, and weather conditions, including clouds and aerosols such as smoke and airborne dust, and also the dew point temperature.

It is clearly not practical to deterministically model realistic weather conditions, especially partly cloudy weather where the sky luminance distribution may vary on a time scale of minutes. Modeling diffuse daylight therefore requires a simplifying mathematical model, which in turn requires measured weather data.

Typical Meteorological Year

There are over 2,100 weather stations around the world (including 1,100 in North America) that measure weather data on an hourly basis. Through a complex set of empirical rules (Wilcox et al. 2008), thirty years or more of weather station data is compared on a per-month basis, and the hourly weather records for the twelve "most typical" months are assembled into a *TYPICAL METEOROLOGICAL YEAR* (TMY3) data set for the station's geographic location[1].

Of the 68 elements in each hourly weather record, two are of primary importance for climate-based daylight modeling:

Element	Unit	Description
Direct normal irradiance	Watt-hour per square meter	Amount of solar radiation received in a collimated beam on a surface normal to the sun during the 60-minute period ending at the timestamp.
Diffuse horizontal irradiance	Watt-hour per square meter	Amount of solar radiation received from the sky on a horizontal surface during the 60-minute period ending at the timestamp.

Direct normal irradiance can be measured with a pyrheliometer, an instrument that measures the solar irradiance (including visible light and ultraviolet and infrared radiation from 300 nm to 2800 nm) incident upon its thermopile sensor (Muneer 2004). The device is always aimed directly at the Sun, and it includes a narrow tube that limits its field of view to six degrees (e.g., Figure 1).

FIG. 1 – Pyrheliometer. (Source: www.hukseflux.com).

Diffuse horizontal irradiance is usually measured with a pyranometer, an instrument (such as that shown in Figure 2) that measures irradiance from the sky incident upon its horizontal thermopile sensor (Muneer 2004). A shadow band may be positioned over the sensor to obscure a six degree-wide band following the path of the Sun, although it must be moved on a regular basis throughout the year. Alternatively (and more accurately), the *GLOBAL HORIZONTAL IRRADIANCE* can be measured without a shadow band, and the measured direct normal irradiance measurement subtracted from it to determine the diffuse horizontal irradiance (*IBID*).

FIG. 2 – Pyranometer. (Source: www.hukseflux.com).

Perhaps surprisingly, these two measurements are all that are needed to model diffuse daylight.

Perez Sky Model

Based on some 16,000 full-sky scans made from Berkeley, California, Perez et al. (1993) proposed an empirical "all weather" sky model that predicts the absolute sky luminance distribution for weather conditions ranging from clear skies to totally overcast. The only two measured input parameters are direct normal and diffuse horizontal irradiance. (The model also includes the dew point temperature as a measure of atmospheric moisture content, but this has only a minor effect on the predicted luminance distribution.)

Other all-weather sky models have been proposed, but various validations studies (e.g., Noorian et al. 2008) have shown that the Perez sky model is better than most. More important, it has been implemented in the *RADIANCE* tool *GENDAYLIT* to generate a single sky luminance distribution, and in *GENDAYMTX* to generate a set of hourly sky luminance distributions for the year from a TMY3 weather data file.

It should also be noted that where TMY3 weather data include direct normal and diffuse illuminance values, they have likely been calculated from the corresponding irradiance measurements using the Perez sky model. When direct normal and diffuse horizontal illuminance values are submitted to *GENDAYLIT*, it uses an undocumented iterative algorithm to estimate the original measured irradiance measurements that the Perez sky model requires.

Sky Luminance Distribution

Prior to the introduction of calibrated all-sky digital cameras with fisheye lenses (e.g., Figure 3), mechanical scanners were used to measure the sky luminance distribution. Still manufactured by EKO Instruments, these instruments consist of a luminance meter mounted on an alt-azimuth platform with stepper motors, and measure the sky luminance at 145 different directions in about 4-1/2 minutes. They were previously used to obtain data for, among other purposes, the validation of various all-weather sky models, including the Perez sky model.

FIG. 3 – Digital all-sky camera. (Source: www.eko-usa.com).

One legacy of these scanners has been the *TREGENZA SKY SUBDIVISION* (Tregenza 1987), wherein the sky dome is subdivided into eight 12-degree horizontal bands with 145 *SKY PATCHES* (Figure 4).

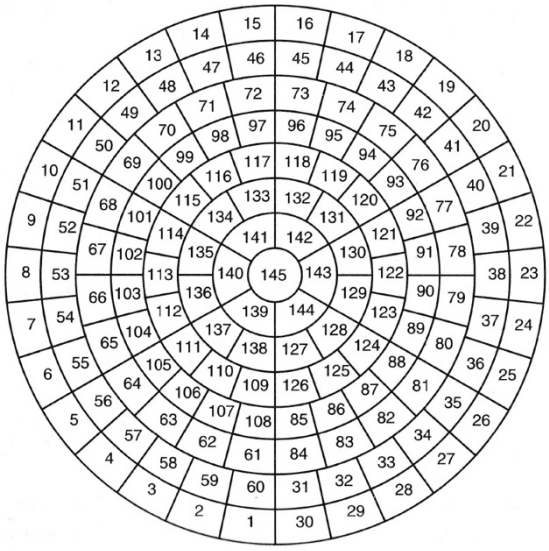

FIG. 4 – Tregenza sky subdivision. (Source: Muneer 2004).

A particular advantage of this subdivision is that the sky luminance distribution can conveniently be represented as 145 discrete luminance values. Apart from the circumsolar region within a few degrees of the solar disk, the luminance of the sky dome in any direction can be interpolated with reasonable accuracy from these values.

Daylight Coefficients

Another advantage of the Tregenza subdivision scheme comes from a paper published over three decades ago, simply titled “Daylight Coefficients” (Tregenza et al. 1983). The researchers observed that each sky patch can be thought of as a separate and independent area light source that potentially illuminates a room through a window or opening (Figure 5). Using radiative transfer theory (aka *RADIOSITY*), they demonstrated that — *IN THEORY* — the luminance distribution in the room due to the intereflection of diffuse daylight from the sky patch (which they called “sky zones”) could be calculated.

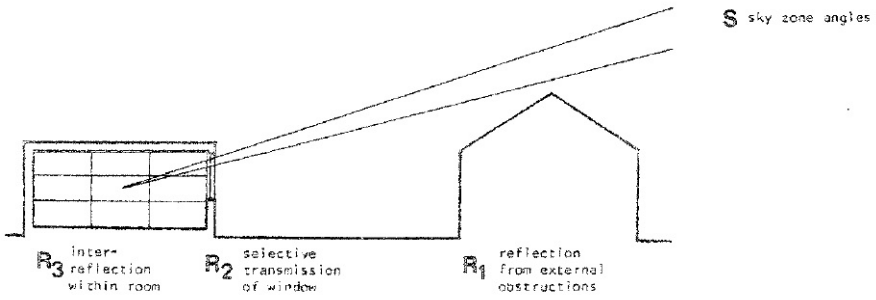

FIG. 5 – Daylight coefficients and sky patches. (Source: Tregenza et al. 1983).

Suppose, then, that each sky patch is assigned a luminance of 1000 cd/m^2. If the luminance distribution in the room due to each patch is calculated and the results summed, the resultant luminance distribution is that due to a uniform sky[2] with a luminance of 1000 cd/m^2. For the lack of any previous terminology, we can call this the *CANONICAL SOLUTION* for the distribution of diffuse daylight in the environment (e.g., Figure 6).

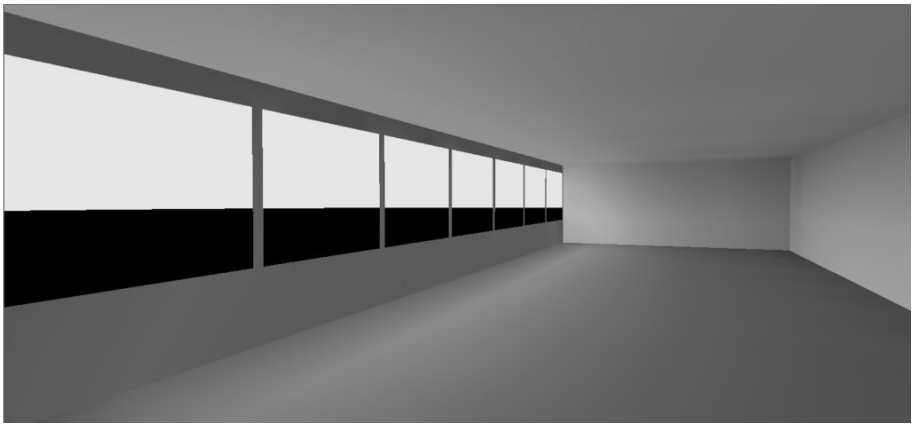

FIG. 6 – Canonical diffuse daylight solution.

Given, however, that each sky patch represents an independent light source, its resultant luminance distribution can be scaled by the average luminance of the sky patch for any given Perez sky model solution and building orientation. Summing these scaled luminance distributions therefore provides the luminance distribution of daylight in the room for the Perez sky model solution (e.g., Figure 7).

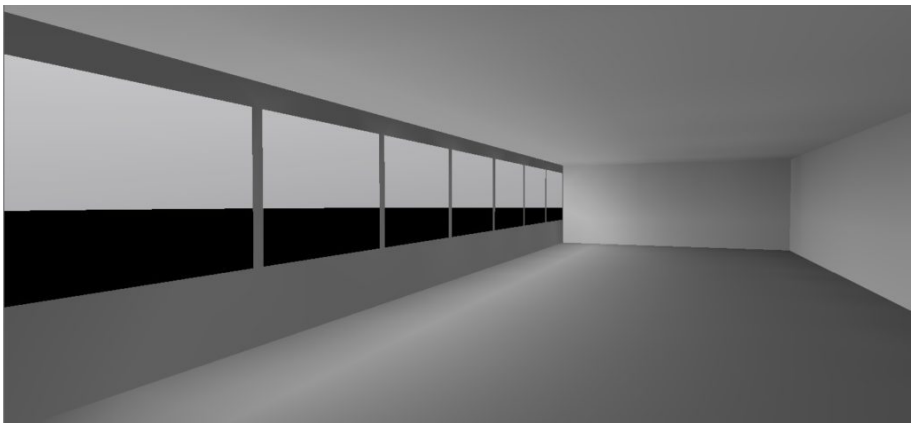

FIG. 7 – Example Perez sky model solution (overcast sky).

THIS IS THE KEY TO CLIMATE-BASED DAYLIGHT MODELING. Given the architectural plans for a building, it is possible to calculate the canonical solution for the distribution of daylight in its rooms and other interior spaces. Then, given a TMY3 or similar weather dataset for the building site, the sky luminance distribution can be calculated for each daylight hour of the year using the Perez sky model, and with this the interior luminance distributions.

The advantage, of course, is that scaling and summing the contributions of each sky patch is much simpler and faster than calculating the canonical daylight solution. Even for complex environments with hundreds of thousands of polygonal elements, this can be done in milliseconds on a commodity desktop computer.

Again, however, this is in theory … in practice, the devil is very much in the details.

Direct Sunlight

The same approach can be applied to direct sunlight. Following an approach proposed by Bourgeois et al. (2008), interior luminance distributions can be calculated for a selected number of solar positions and included with the canonical solution (although they do not appear in the renderings). For a given TMY3 weather record, the solar position can then be calculated and the direct sunlight contribution bilinearly interpolated from the luminance distributions of the four closest precalculated solar positions.

Bourgeois et al. (2008) proposed that 65 solar positions chosen at hourly intervals on five selected days would be sufficient (Figure 8). However, choosing 120 solar positions at hourly intervals on nine selected days (Figure 9) is arguably a better choice. In particular, the average separation between solar positions is eight degrees, and the maximum separation is ten degrees. While a difference of four to five degrees may be significant in calculating the direct sunlight distribution in interior spaces for static scenes (and particularly so for photorealistic renderings), it is likely acceptable for climate-based daylight modeling where the sun traverses 15 degrees of the sky between hourly weather records. (It must also be remembered that each hourly weather record represents the average direct normal and diffuse horizontal irradiances measured over the previous hour.)

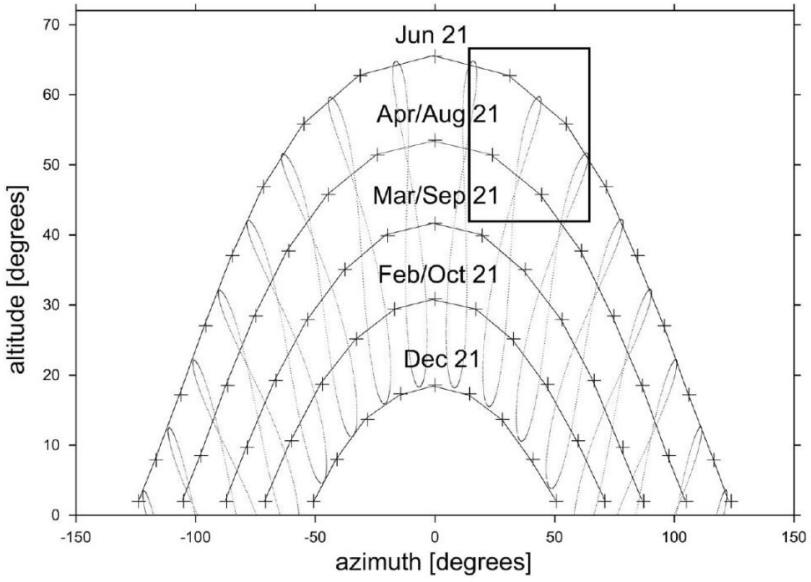

FIG. 8 –Annual solar path (65 positions) for Freiberg, Germany. (Source: Bourgeois et al. 2008).

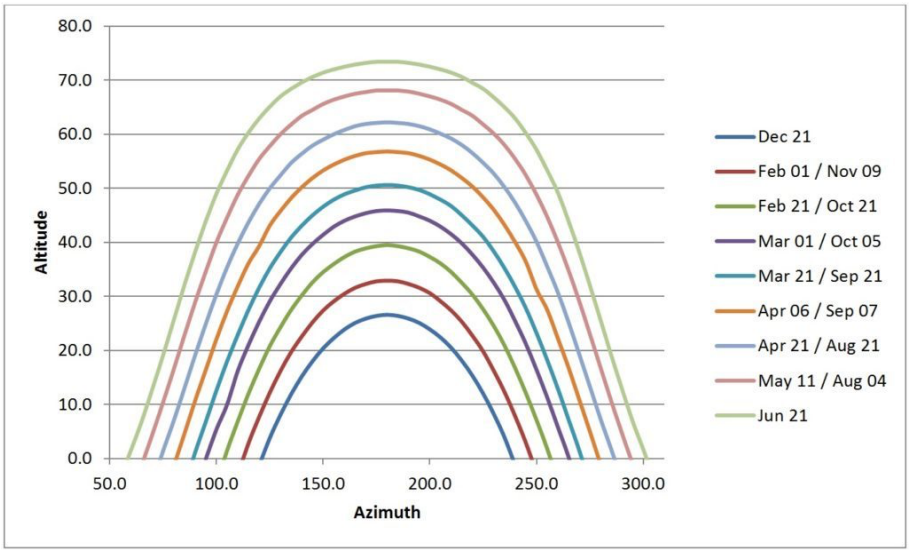

FIG. 9 – Annual solar path for Boulder, Colorado.

An example interior luminance distribution, including both diffuse daylight and direct sunlight, is shown in Figure 10. It should be noted that unlike ray-traced images, the shadow edges are not sharply defined. This is due to the mesh spacing of the floor (in this case 0.2 meters), and it is intentional. (This issue will be addressed in greater detail further on in this article.)

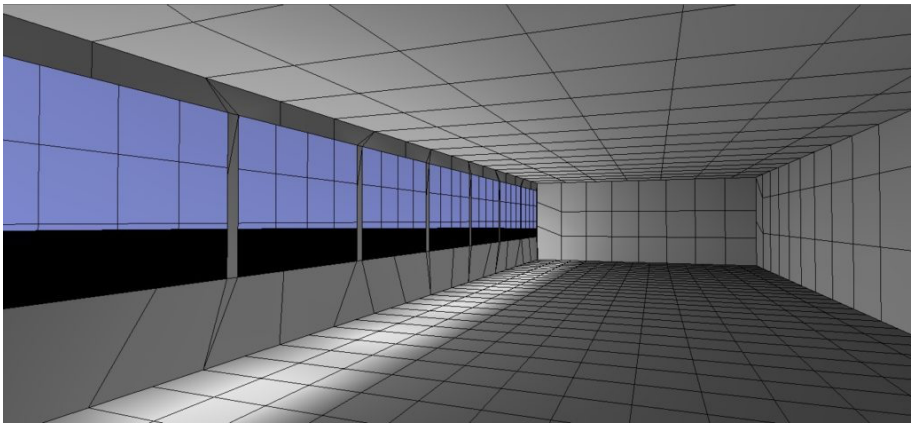

FIG. 10 – Example Perez sky model solution (clear sky).

Ground Reflections

Direct sunlight and diffuse daylight reflected from the ground must also be taken into account, even if the architectural model does not include exterior surfaces. This can be accomplished by modeling a *VIRTUAL GROUND PLANE* as an inverted sky dome (a *GROUND DOME*) with the same number of *GROUND PATCHES* (Figure 11). Each ground patch serves the same purpose as its corresponding sky patch as an area light source. Unlike sky patches, however, all ground patches have the same luminance because they are diffusely reflecting light from the entire sky dome.

Assuming that the average reflectance of outdoor scenes is 18 percent (the same as a photographic gray card), the luminance of all ground patches is equal to 18 percent of the horizontal illuminance. Therefore, only a single interior luminance distribution needs to be determined for exterior ground reflections, which is included with the canonical solution and subsequently scaled according to the horizontal irradiance for a given TMY3 weather record.

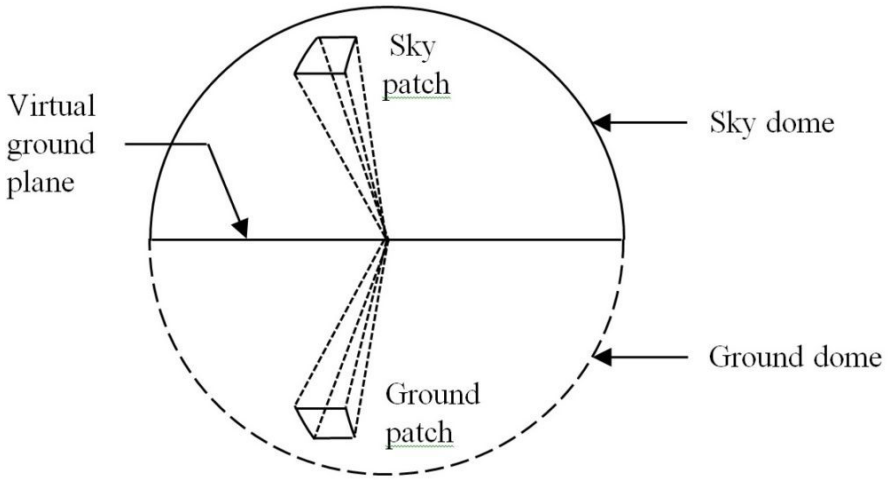

FIG. 11 – Sky dome and inverted ground dome.

Sky Dome Discretization

Yet another detail: most radiosity methods require all surfaces to be represented as meshes of triangular and quadrilateral elements. This is problematic in terms of the Tregenza sky subdivision, whose sky patches have curved edges. If the sky dome is represented as planar trapezoidal elements (e.g., Figure 12), the resultant gaps will result in errors of several percent or more when calculating luminance distributions due to diffuse daylight.

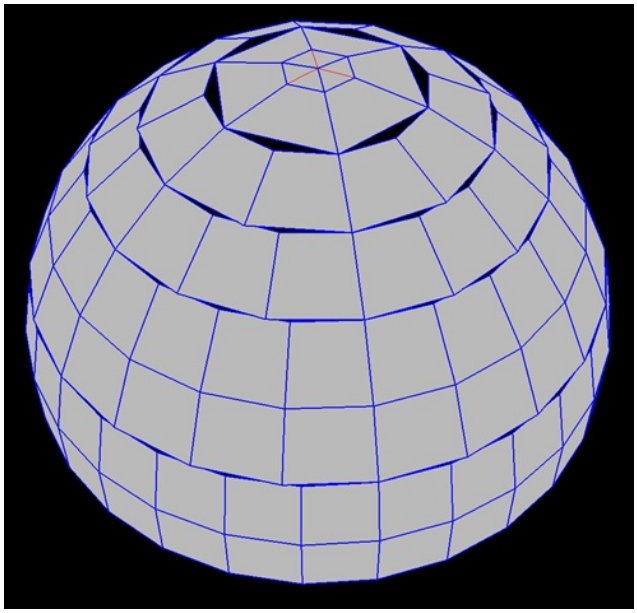

FIG. 12 – Tregenza sky subdivision errors.

The solution is to instead represent the sky dome with a hemispherical geodesic dome. The vertex coordinates of each planar sky patch can be determined by recursively subdividing half of an octahedron, as shown in Figure 13. Three subdivisions result in a geodesic dome with 256 triangular (and, of course, planar) patches with no gaps.

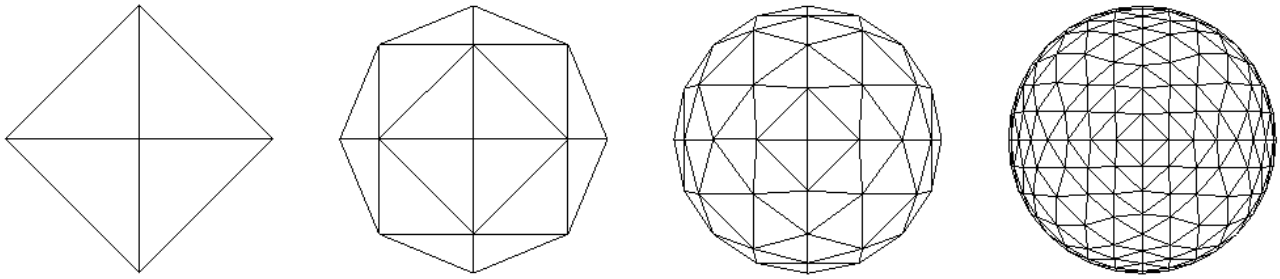

FIG. 13 – Octahedron subdivision.

With this, there is another important detail to consider. In their "Daylight Coefficients" paper, Tregenza et al. (1983) assumed that each sky patch would be projected onto a point on each surface element in the environment, as shown in Figure 5. This works in theory, but it is computationally inefficient in the extreme in that all 256 sky patches would need to be projected onto each surface element of both the interior and exterior environments. With today's architectural models, this could involve hundreds of thousands of elements … and hours to days of computer time (e.g., Muller et al. 1995).

Parallel Sky Patch Projection

A much more efficient approach is to model each sky patch like the solar disk, as an infinitely distant point source that produces a parallel beam of light (Ashdown 2004). With this, the sky patch illumination can be projected onto the entire environment at once, with all surface elements being considered in parallel (Figure 14). This is a standard computer graphics operation that can be performed either in software (e.g., Ashdown 1994) or in hardware using the computer's graphics processing unit (Rushmeier et al. 1990).

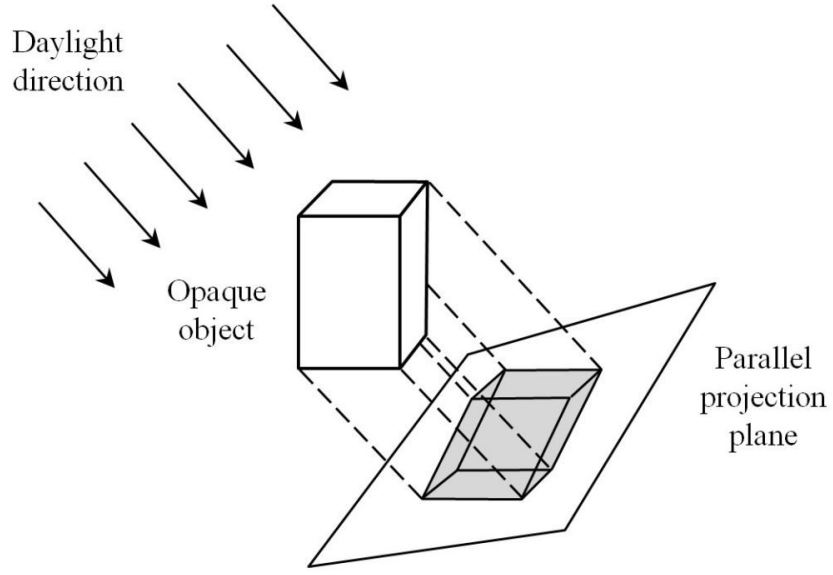

FIG. 14 – Parallel sky patch projection.

This approach works well for most exterior environments because the envelopes of exterior objects (such as buildings) are typically convex. As a result, each exterior surface element is visible to multiple sky patches, with their parallel light beams being averaged and so not noticeable in the computer graphics renderings.

This assumption fails, however, for the windows and openings of interior environments. An example is presented in Figure 15, where the parallel light beams from the discrete sky patches are clearly visible as light “spokes” when they are projected through a narrow window onto the surfaces of interior environment.

Another problem (not illustrated here) is that the light levels in interior environments are often orders of magnitude less than the exterior horizontal illuminance. When the CAD models (such as the simple box shown in Figure 15) are specified, their surface edges may align exactly. However, when these models are rotated, translated, and possibly scaled in world space coordinates for lighting calculations, floating-point round-off of the vertex coordinates may result in very small gaps between surfaces such as the walls and floor.

(This is not a software problem — it is basically impossible to avoid this problem. Even the most high-end computer graphic displays may exhibit occasional single-pixel flickering at the surface edges when the objects are rotated or orbited for viewing.)

Even though the gaps may be fractions of a millimeter wide in world space, they allow direct sunlight or even diffuse daylight to enter the interior environment. While the amount of light is usually insignificant in terms of lighting calculations, the resultant “light leaks” can be quite obvious in computer graphics renderings.

To address these two problems, a radically different approach is needed when handling windows and openings in daylight calculations.

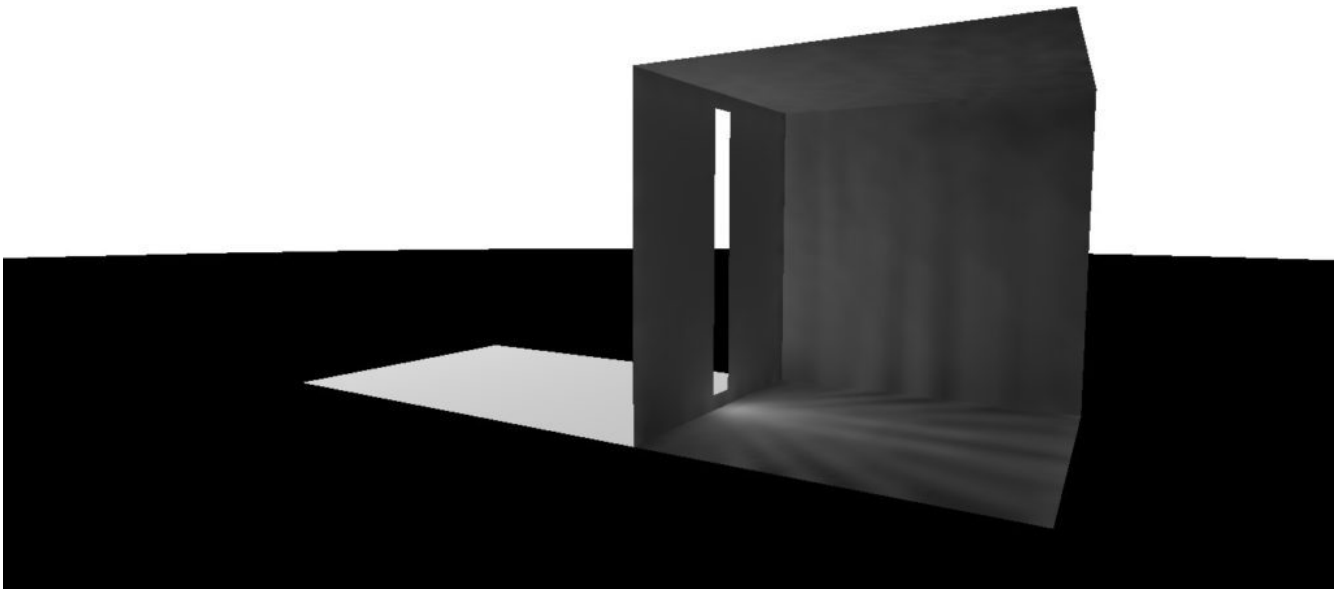

FIG. 15 – Light “spokes” due to parallel beams from discrete sky patches.

Windows and Openings

As previously noted, each exterior surface element is visible to multiple sky patches, with their parallel light beams being averaged. Windows are no different — they typically have a full hemispherical view of the exterior environment. Imagine then placing a camera with a fisheye lens facing outwards on the window and capturing a hemispherical image of the visible sky patches and exterior surface elements.

Comparing this to a ray tracing approach, each pixel represents a light ray that is incident upon the camera. It is slightly better than this, as the pixels each "see" a rectangular cone of light with no gaps between them. This being done in software, the camera resolution is arbitrary. With (say) 1.5 million pixels, a highly detailed high dynamic range image can be captured. The value of each pixel is the red-green-blue spectral *RADIANCE* [3] in its field of view.

If we now reverse the camera orientation such that it faces inwards, we can project this HDR image onto the interior surface elements. This effectively transfers diffuse daylight and direct sunlight through windows and openings without the problems of light spokes, as shown in Figure 16.

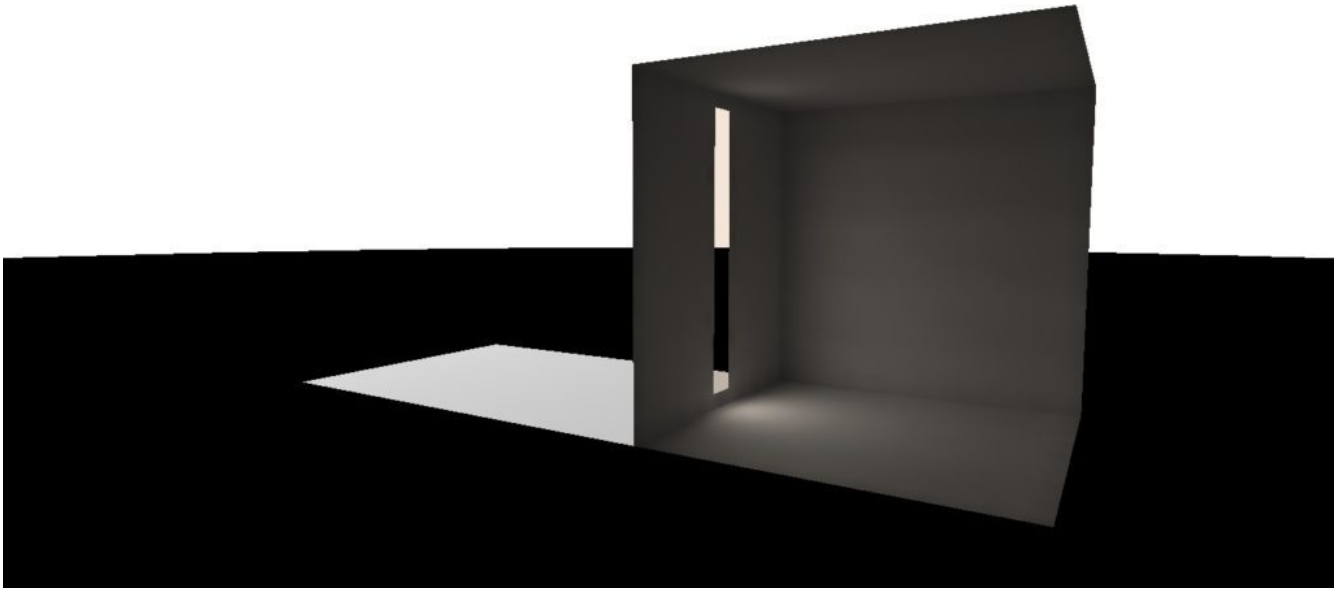

FIG. 16 – Virtual cameras on windows eliminates light spokes.

The virtual camera measures the exterior spectral radiance distribution at its position on the window. At the same time, the projection of the parallel light beams from the sky patches yields the average spectral irradiance of the entire window surface. Knowing this value and the window area, the total amount of spectral radiant flux that is to be transferred through the window can be calculated. There are, of course, further details — many of them — that need to be considered with this approach. Glass windows and transparent plastic (collectively, dielectric) surfaces exhibit complex reflectance and transmittance characteristics that vary with incidence angle (described by Fresnel equations), and may also exhibit spectrally selective absorptance (e.g., colored glass). There may also be multiple surfaces (e.g., triple-pane glazing) present. All of these issues, however, can be efficiently dealt with using radiosity-based methods.

This approach addresses the light spokes issue, but not light leaks due to floating-point round-off of the environment geometry. Solving this problem requires that the environment be separated into "exterior" and "interior" surfaces. The difference is that interior surfaces are illuminated only by daylight that is transferred through windows and openings (collectively, *TRANSITION* surfaces). With this approach, light leaks can be completely eliminated, no matter how imprecise the environment geometry.

Eliminating Hot Spots

There is yet another problem to consider. If we place the virtual camera at the center of a large window that is too close to an interior surface, it may result in a "hot spot" on the surface (e.g., Figure 17).

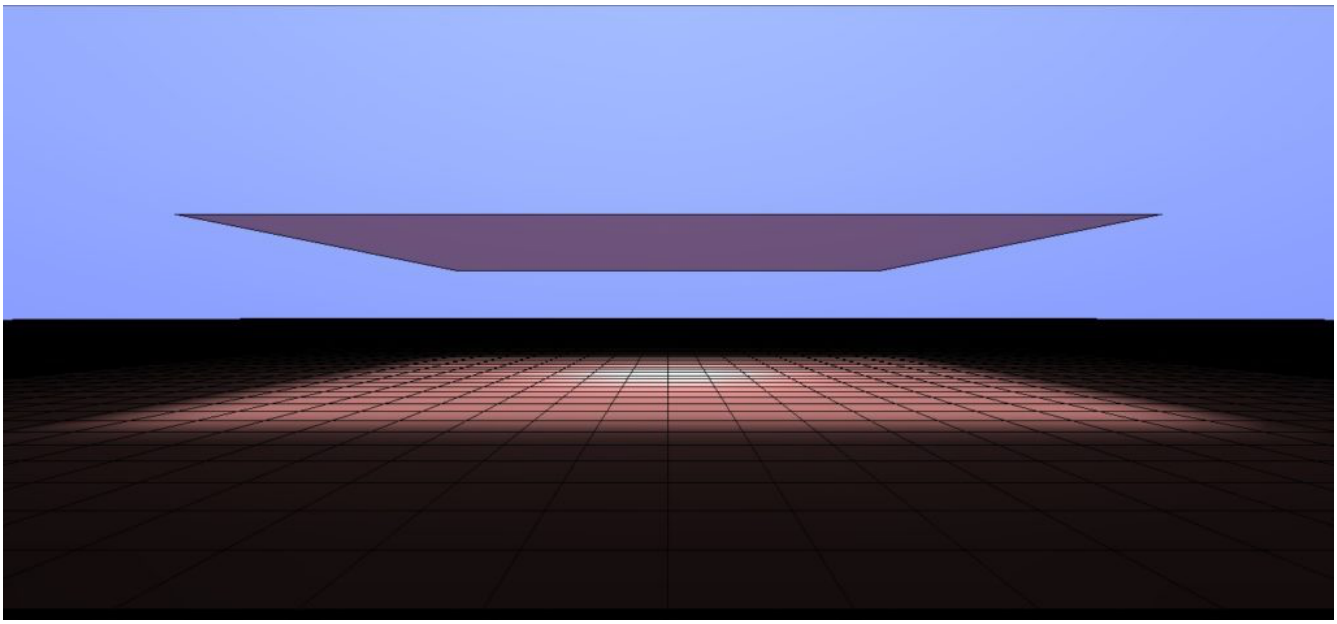

FIG. 17 – Single window patch results in "hot spot" on interior surface.

The reason for this spot is clear: the camera is concentrating all the light received by the window at a single point and projecting it onto the surface. The window is being modeled as a point source, and so the inverse square law applies.

The solution is equally clear, and in fact is required by IES LM-83-12: model large windows as an array of 0.3-meter square window "patches" (IES 2012). As long as the nearest significantly large interior surface is at least 0.6 meters distant (or twice the width of each window patch), the problem of hot spots will be eliminated (e.g., Figure 18).

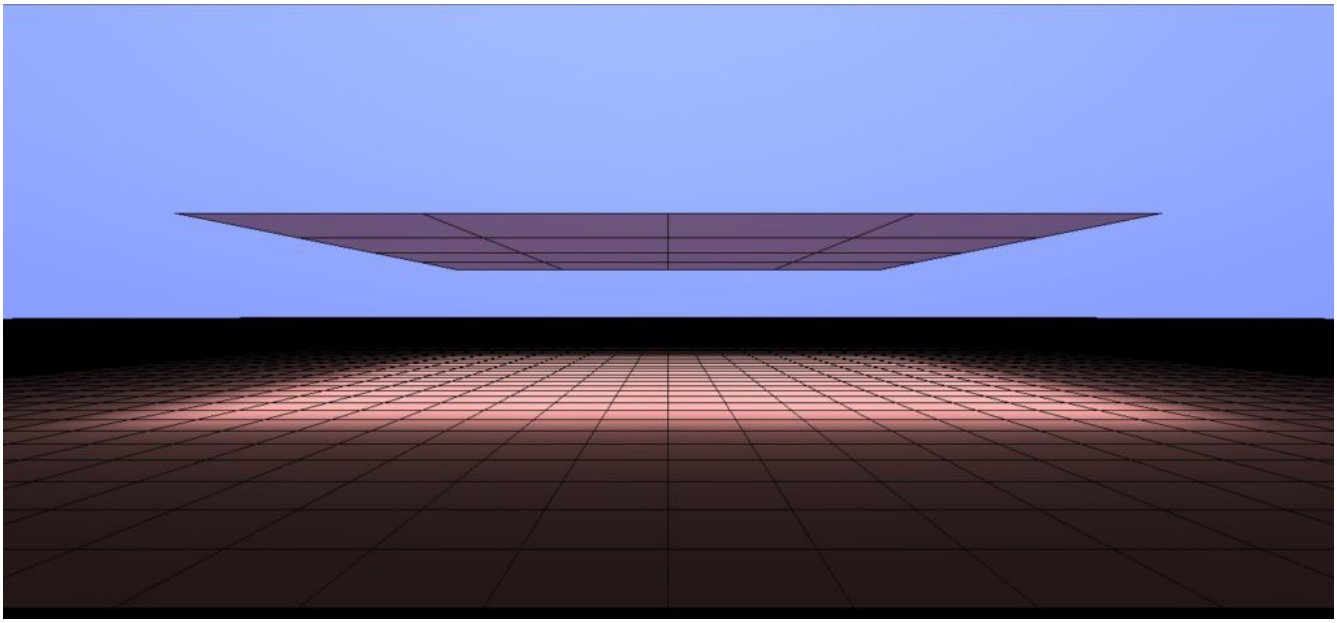

FIG. 18 – Multiple window patches eliminate hot spots.

Annual Daylight Simulations

Without delving into the details of how the radiosity method works — see Ashdown (1994) for some 500 pages of explanation — roughly 95 percent of the calculation time involves computing form factors between surface elements for each "step" of the iterative radiosity solution (e.g., Rushmeier et al. 1990). Most of the remaining time per step is spent calculating the amount of light transferred between elements with each "bounce" of light.

With the radiosity method, each surface element is assigned a parameter that represents how much light (technically, *SPECTRAL RADIANT EXITANCE*) it has received at each step in the calculations. Given that there are 256 sky patches, 120 solar positions, and a virtual ground plane, all that needs to be done (while blithely ignoring the myriad details) is to assign an additional 377 parameters per surface element. These are used to store the 377 separate radiosity solutions that together represent the canonical daylight solution for the environment. This requires a considerable but still manageable amount of memory for even complex environments.

The same approach can be applied to electric lighting channels, with one additional parameter per channel. This enables, for instance, the ability to model daylight harvesting systems with switched or dimmable luminaires.

The obvious question is, how quickly can these calculations be performed, particularly for complex environments with tens to hundreds of thousands of surface elements? While these are clearly empirical results, numerous experiments to date have shown that it takes between two and three times as long to calculate a canonical solution as it does to calculate an equivalent static radiosity solution for a specific date and time.

… but the devil still remains in the details …

Transition Surfaces

Looking again at the virtual cameras used to capture images of the exterior environment and project it onto the interior environment, it can be seen that each pixel needs to represent 377 spectral radiance values per pixel. Assuming a 1.5 megapixel image, this represents at least several gigabytes of memory. With a multithreaded program simultaneously processing eight to sixteen cameras, it is clear that the virtual camera approach will fail spectacularly.

The solution to this problem, however, is simple: assign a unique identifier to each surface element, which is then assigned to the pixels that "see" it in the virtual image. When the image is projected onto the interior surface elements, the identifiers can be used to access the exterior surface elements and their canonical solution values.

Looking more closely at windows and openings, Figure 19 diagrammatically shows virtual cameras positioned at the centers of multiple window patches, where each camera captures a hemispherical image of the exterior environment and projects the image into the interior environment.

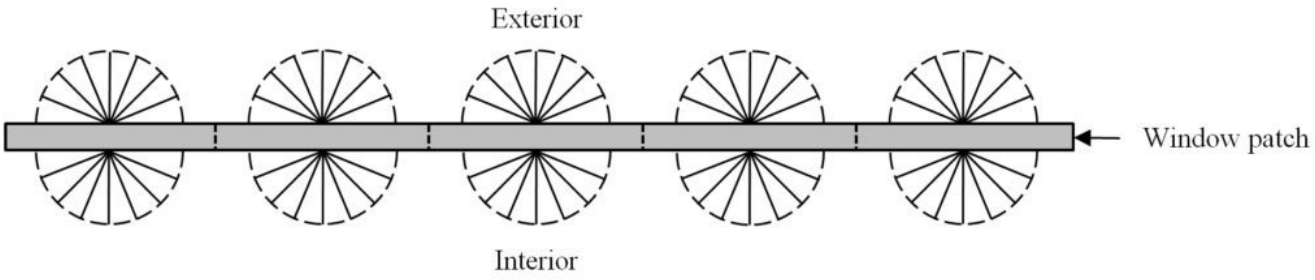

While this approach clearly works (e.g., Figure 18), it is computationally demanding. With complex architectural models such as buildings with hundreds of windows and potentially thousands of virtual cameras, the calculation times could extend into hours.

With this, it is instructive to consider again the observation that the image is equivalent to tracing a million or more rays through the camera position. With (say) a large window subdivided into one hundred 0.3-meter square window patches, this represents a dense array of 100 million light rays emanating from a single window. This may be necessary because the interior surfaces are relatively close to the window, and so the window patches are needed to avoid the formation of hot spots. For the exterior environment, however, there may not be any similarly close surfaces, and so a single virtual camera positioned in the center of the window is sufficient to capture the hemispherical image (e.g., Figure 20).

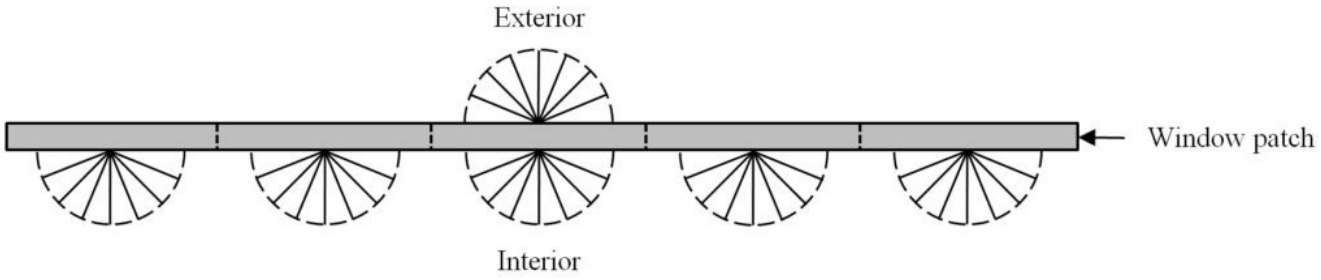

FIG. 20 – Single virtual camera positioned on window exterior.

By itself, this does little to reduce the computational burden of tracing perhaps 100 million rays per window. In practice, however, as few as one million rays are likely sufficient (especially when it is considered that each ray is actually a finite width cone rather than an infinitesimally narrow ray). The solution to this problem is to first capture the exterior image, and then randomly assign each of its pixels (i.e., rays) to one of the multiple cameras projecting the image into the interior environment. This has the effect of distributing the projected rays across the interior side of the window, which is needed to prevent the formation of hot spots. At the same time, the number of rays that need to be traced is reduced to those of a single virtual camera.

This process can be made adaptive, because each image pixel also provides the distance from the camera to the first intersected surface. By first capturing and projecting an image from the center of the window, this depth information can be used to identify the closest surfaces and so decide how best to subdivide the window on both sides (exterior and interior) for camera placement.

As complicated as this may look, it is computationally efficient. As an example, the environment shown in Figure 10 required 28 seconds of calculation time on a commodity desktop computer when calculated as a static environment for a given time and date. It is a simple environment with only 800 surface elements, but most of the calculation time is spent on transferring the direct sunlight and diffuse daylight through 84 window patches.

By comparison, the canonical solution shown in Figure 6 required only 42 seconds of calculation time. Once completed, any of the 4,380 hourly weather records in the TMY3 weather data can be calculated and displayed in milliseconds.

Bidirectional Transmittance Distribution

One of the criticisms of the radiosity approach for daylight simulation is that it can only model diffuse reflections. Quoting IES RP-5-13, Recommended Practice for Daylighting Buildings (IES 2013):

> *RADIOSITY METHODS ASSUME THAT ALL SURFACE MATERIALS HAVE PERFECTLY DIFFUSE REFLECTANCE, I.E., THEY REFLECT LIGHT EQUALLY IN ALL OUTGOING DIRECTIONS FOR ALL INCIDENT ANGLES OF INCOMING RADIATIONS.*

This was a true statement when radiosity methods were first developed in the late 1980s, but it is certainly not true today. Radiosity methods are capable of accurately modeling the optical and spectral properties of opaque, transmissive, and translucent surfaces, including Fresnel reflectance and transmittance. They are also capable of accurately modeling both isotropic and anisotropic bidirectional reflectance and transmittance distribution functions (BRDFs and BTDFs) using analytic functions or measured data represented by the LBNL bidirectional scattering distribution's function (BSDF) data format (once its specification has been finalized and published).

If commercial lighting design software has yet to support all of this functionality, it is only because there has been insufficient demand to date. IES LM-83-12 (IES 2012), however, specifies the modeling of window shades and blinds using their BSDF properties *IF AVAILABLE*. Once this information become widely available from manufacturers, its simulation for CBDM purposes can be supported.

There is, however, no need to wait for measured BSDF data to become available in order to comply with the requirements of LM-83-12. Apart from advanced fenestration devices that redirect light, most diffusing glazings and fabric window shades behave as simple diffusers. Given a virtual camera, it is straightforward to include a virtual diffusion filter to model these glazings and shades.

Figure 21 illustrates several example window bidirectional transmittance distributions at incidence angles ranging from 20 to 60 degrees, and with three different degrees of diffusion. These would normally be applied to the direct sunlight entering an interior environment, but the same approach can be applied to light redirection devices such as semispecular light shelves.

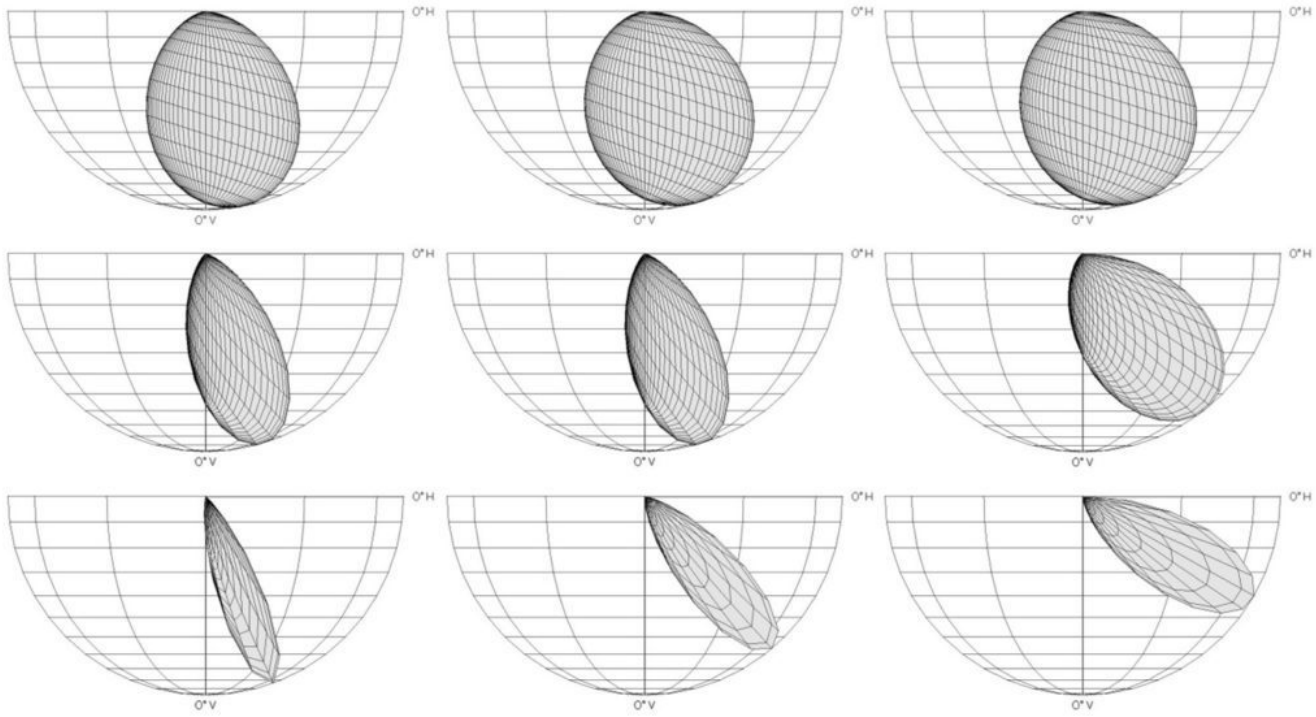

FIG. 21 – Example window bidirectional transmittance distributions.

It is equally straightforward — in principle — to define a BSDF "filter" in software for the virtual camera that will redirect incident rays such that they are either transmitted or reflected by the window or other designated surface. This, however, is a work in progress for the radiosity approach.

Virtual Photometers

There is no point in calculating the distribution of daylight within an interior environment if it cannot be measured for daylight metric calculations and other purposes. Perhaps surprisingly, this is where radiosity-based CBDM has a distinct advantage over ray tracing methods.

The original radiosity methods only provided illuminance and luminance measurements for selected points on opaque surfaces after the radiosity calculations had been completed. However, it possible to extend these methods such that transparent surfaces can be specified that receive but do not

otherwise influence the flow of light within the environment. By subdividing these surfaces, each surface element becomes a virtual photometer (e.g., Figure 22).

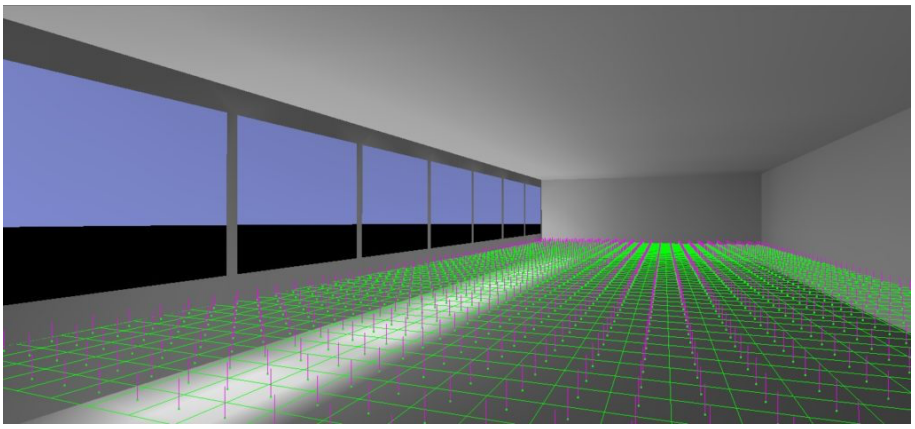

FIG. 22 – Virtual photometers.

The advantage of these photometers is that they record all the light passing through them in one direction — which is exactly what is needed when performing most daylight metric calculations. By comparison, an array of photometers used in ray-traced CBDM calculations will only measure the light incident at each meter position. Depending on the resolution of the direct sunlight shadows cast by Venetian blinds, for example, those meters that are shadowed may result in the spatial Daylight Availability (sDA) and Annual Sunlight Exposure (ASE) values being underreported.

Another advantage of these photometers is that they are computationally efficient. In the above example, there are 800 surface elements and 1,500 virtual photometers placed on an imaginary workplane. Where it took 42 seconds to calculate the canonical solution without the photometers, it took 57 seconds with them. Again, this is for the canonical solution — calculating the meter values for a given TMY3 weather record is a matter of a few more milliseconds.

Looking Forward

Much of the above has been developed specifically for climate-based daylight modeling using radiosity methods. It has been implemented in commercial lighting design software, but there will undoubtedly be minor changes as users gain experience with its features and capabilities.

There are also opportunities for further improvements and optimizations, but these will not be discussed until the research and development work has been completed ñ hopefully in less time than the twelve years it has taken to reach this point!

To date, climate-based daylight modeling has relied on ray tracing methods, specifically *RADIANCE* and its derivatives. There is nothing wrong with this, other than that it has possibly hindered research into alternative approaches.

This, however, is symptomatic of a larger issue. With software products such as *LIGHTSCAPE* in the early 1990s, radiosity methods were favored for Hollywood's computer graphics requirements. However, the introduction of photon mapping techniques (Jensen 2001) and vastly increased computing power through "rendering farms" (thousands of dedicated computers on a network), followed by techniques such as multidimensional light cuts and Metropolis light transport, soon eclipsed radiosity methods.

Research into radiosity methods peaked in 1994 and has been declining ever since, as evidenced by the yearly total of academic papers on the topic shown in Figure 23. It is, in the terminology of computer scientists, a "solved problem."

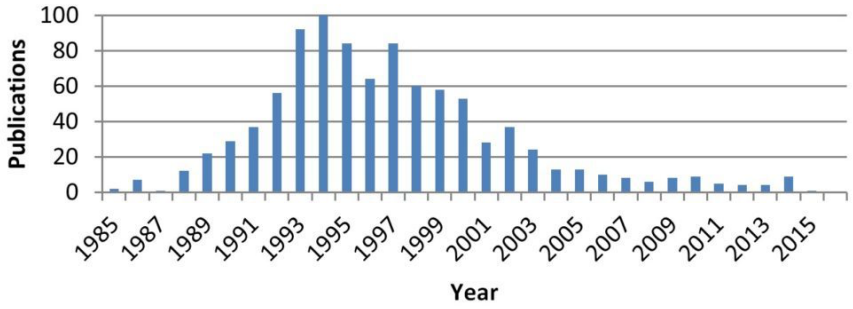

Fig. 23 – Radiosity papers publication frequency.

As this article has attempted to show, however, there is still life to be had in radiosity methods. As the humorist Mark Twain famously never said, "The reports of my death have been greatly exaggerated."

Acknowledgements

Thanks to Dawn De Grazio of Lighting Analysts Inc. for her review and comments on this article.

References

Ashdown, I. 1994. Radiosity: A Programmer's Perspective. New York, NY: John Wiley & Sons.

Ashdown, I. 2004. "Modeling Daylight for Interior Environments," *2004* IESANZ Annual Conference Proceedings, Illuminating Engineering Society of Australia and New Zealand.

Bourgeois, D., C. F. Reinhart, and G. Ward. 2008. "Standard Daylight Coefficient Model for Dynamic Daylighting Simulations," Building Research & Information 36(1):68-82.

CIE. 2003. Spatial Distribution of Daylight — CIE Standard General Sky, CIE Standard S 011/E:2003. Vienna, Austria: CIE Central Bureau.

IES. 2010. IES Lighting Handbook, Tenth Edition. New York, NY: Illuminating Engineering Society.

IES. 2012. LM-83-12, IES Spatial Daylight Autonomy (sDA) and Annual Sunlight Exposure (ASE). New York, NY: Illuminating Engineering Society.

IES. 2013. RP-5-13, Recommended Practice for Daylighting Buildings. New York, NY: Illuminating Engineering Society.

Jensen, H. W. 2001. Realistic Image Synthesis Using Photon Mapping. Natick, MA: A. K. Peters.

Mardaljevic, J. 2006. "Examples of Climate-Based Daylight Modeling," Paper No. 67, CIBSE National Conference 2006: Engineering the Future.

Müller, S., W. Kresse, N. Gatenby, and F. Schaffel. 1995. "A Radiosity Approach for the Simulation of Daylight," Rendering Techniques '95 (Proceedings of the Sixth Eurographics Workshop on Rendering), pp. 137-146. New York, NY: Springer-Verlag.

Noorian, A. M, I. Moradi, and G. Kamali. 2008. "Evaluation of 12 Models to Estimate Hourly Diffuse Irradiation on Inclined Surfaces," Renewable Energy 33:1406-1412.

Muneer, T. 2004. Solar Radiation and Daylight Models, Second Edition. Oxford, UK: Elsevier Butterworth-Heinemann.

Nabil, A., and J. Mardaljevic. 2006. "Useful Daylight Illuminances: A Replacement for Daylight Factors," Energy and Buildings 38(7):905-913.

Perez, R., R. Seals, and J. Michalsky, 1993. "All-Weather Model for Sky Luminance Distribution – Preliminary Configuration and Validation," Solar Energy 50(3):235-245.

Rushmeier, H. E., D. R. Baum, and D. E. Hall. 1990. "Accelerating the Hemi-Cube Algorithm for Calculating Radiation Form Factors," ASME Journal of Heat Transfer 113:1044-1047.

Tregenza, P. R., and I. M. Waters. 1983. "Daylight Coefficients," Lighting Research and Technology 15(2):65-71.

Tregenza, P. R. 1987. "Subdivision of the Sky Hemisphere for Luminance Measurements," Lighting Research and Technology 19:13-14.

2013. LEED v4 BD+C: Schools — Daylight. Washington, DC: U.S. Green Building Council (www.usgbc.org).

Wienold, J., and J. Christoffersen. 2006. “Evaluation Methods and Development of a New Glare Prediction Model for Daylight Environments with the Use of CCD Cameras,” Energy and Buildings 38:743-757.

Wilcox, S., and W. Marion. 2008. User’s Manual for TMY3 Data Sets. Technical Report NREL/TP-581-43156, Revised May 2008.Golden, CO: National Renewable Energy Laboratory.

[1] The World Meteorological Organization (www.wmo.int) defines “climate” as the “average weather” over a period of thirty years. The weather at a given location will of course vary on a per-year basis — sometimes drastically — from that of the Typical Meteorological Year weather data for that location.

[2] A uniform sky luminance distribution is equivalent to CIE Standard General Sky Type 5 (CIE 2003).

[3] Spectral radiance in this context refers to representing visible light as a combination of red, green, and blue (RGB) light. Assuming a 6500K light source, the equivalent luminance value L is given by L = 0.2125 * R + 0.7154 * G + 0.0721 * B.

Light Pollution Information

MOBILE LIGHT POLLUTION

Ian Ashdown, P. Eng., FIES, Senior Scientist, SunTracker Technologies Ltd. Published: 2016/01/21

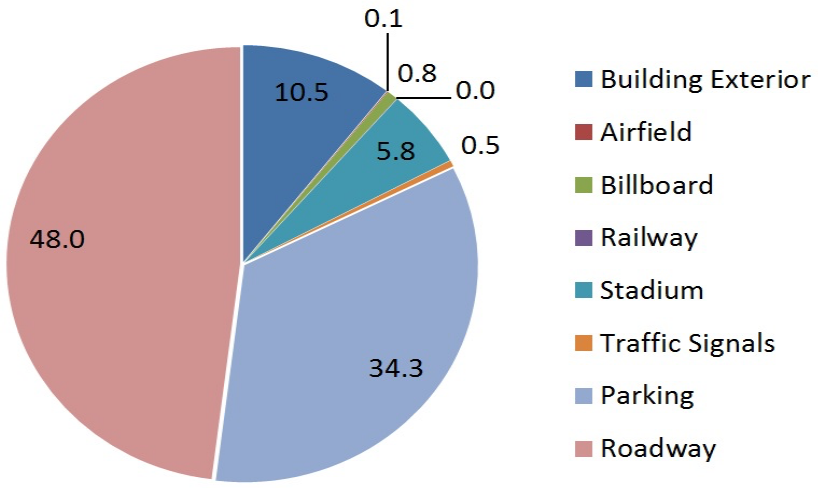

At first glance, this appears to be an innocuous question:

HOW MUCH LIGHT POLLUTION IS ATTRIBUTABLE TO AUTOMOTIVE HEADLIGHTS?

It is also a good question in that if we are to address light pollution, we need to know what causes it. For this, we first need to look at the U.S. Department of Energy publication, *2010 U.S. LIGHTING MARKET CHARACTERIZATION* (DOE 2010).

Section 4.2.4, *OUTDOOR RESULTS*, tabulates the estimated number of outdoor lamps and their wattages nationwide by application in Tables 4.27 and 4.28 (Fig. 1), while Table C.2, *SYSTEM EFFICACY ASSUMPTIONS*, tabulates the lamp efficacies (Table 1).

Table 4.27 Estimated Inventory of Outdoor Lamps by Subsector (1,000's)

	Incandescent	Halogen	CFL	Linear Fluorescent	MV	MH	HPS	LPS	LED	Other	Total
Building Exterior	14,775	2,621	12,052	12,468	1,815	9,865	7,919	274	1	294	**62,084**
Airfield	414	512							98		**1,024**
Billboard				5	5	502			7		**519**
Railway	549								427		**976**
Stadium		64			7	839	120				**1,030**
Traffic Signals	785								14,908		**15,693**
Parking	992	824		16,595	429	14,191	14,205		2,231	2,701	**52,168**
Roadway	300		2	55	1,922	4,116	35,698	1,182	1,546	61	**44,882**
Total	**17,815**	**4,021**	**12,054**	**29,123**	**4,178**	**29,513**	**57,942**	**1,456**	**19,218**	**3,056**	**178,376**

Table 4.28 Average Wattage per Lamp by Subsector in 2010

	Incandescent	Halogen	CFL	Linear Fluorescent	MV	MH	HPS	LPS	LED	Other	Average
Building Exterior	61	74	22	42	79	72	78	74	28	68	55
Airfield	92	65							17		71
Billboard				148	400	400			125		394
Railway	18								14		16
Stadium		4375			1,000	1,554	1,000				1,661
Traffic Signals	130								9		15
Parking	112	108		73	350	224	201		60	97	153
Roadway	181		44	50	243	233	230	78	71	62	221
Average	**68**	**148**	**22**	**60**	**185**	**215**	**204**	**77**	**20**	**93**	**132**

Fig. 1 – Estimated inventory of outdoor lamps. (Source: DOE 2010).

Lamp Type	Luminous Efficacy (lm/W)
Incandescent	12.2
Halogen	16.5
CFL	54.6
Linear Fluorescent	73.7
Mercury Vapor	30.5
Metal Halide	60.0
High Pressure Sodium	83.6
Low Pressure Sodium	89.2
LED	45.3
Other	75.8

Table 1 – System efficacy assumptions. (Source: DOE 2010).

With this information, we can estimate the relative lamp lumens per application (Fig. 3):

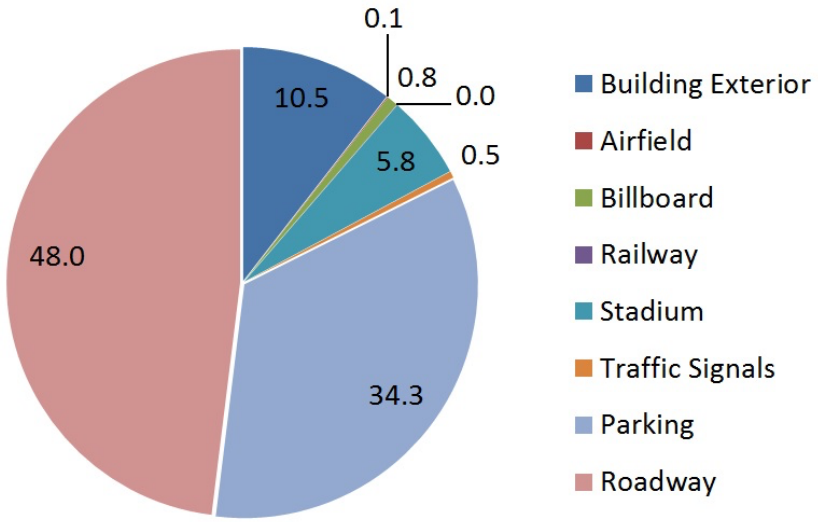

Fig. 3 – Relative lamp lumens by application. (Source: DOE 2010).

The interesting thing about this chart is that while the mix of lamp types has changed markedly since 2010 — LEDs are rapidly replacing high-pressure sodium (HPS) and metal halide (MH) lamps in roadway applications, for example — the relative lamp lumens by application should remain relatively constant[1].

With this, we can see that roadway lighting, outdoor parking lots, building exterior lighting, and stadium lighting contribute the most to light pollution on a per-lumen basis. Billboards (0.8 percent) and airfields (0.1 percent) may significantly impact surrounding residential neighborhoods, but they are mostly insignificant once you get outside of urban centers to dark-sky observing sites.

Automobiles

What the *2010 U.S. LIGHTING MARKET CHARACTERIZATION* report does not address, of course, is automotive lighting, specifically headlamps. For this information, we have to go in search of data in order to synthesize an answer.

According to Wikipedia, the most common types of headlamps in North America are HB1/9004 dual-filament tungsten-halogen lamps, which generate 700 lumens, and high-intensity discharge (HID) lamps, which generate 2,800 to 3,500 lumens, both on low-beam. To this, we can add a growing number of LED and, in the future, laser headlamps.

Going forward, however, it is reasonable to assume that the average lumen output of an automotive headlamp will be approximately 3,000 lumens, giving 6,000 lumens per vehicle.

In calculating light pollution using various mathematical models such as those by Garstang (1986) and Aubé (2015), it is commonly assumed that the average person in urban environments requires between 1,000 and 1,500 lumens of outdoor lighting (i.e., per capita). At 6,000 lumens per vehicle, it is then reasonable to ask whether motor vehicles, including automobiles, contribute to light pollution.

The next part of the question is to ask how many vehicles there are per capita.

Again, Wikipedia provides an answer: in the United States, there are 0.809 vehicles per capita. (As a curious aside, the miniscule microstate of the Most Serene Republic of San Marino has 1.263 vehicles per capita — over 41,000 of them in a country of 24 square miles that is surrounded by a relatively impoverished Italy.)

Now, however, comes the difficult part of the question: how many of these vehicles are on the road at any given time? This is not an easy question to answer. A common metric for transportation planners and engineers is the Annual Average Daily Traffic (AADT). This is determined in principle by counting all the vehicles on a highway or road for a year and then dividing by 365 days.

In practice, it is costly to install and maintain permanent automated traffic counters, and so portable automatic counters (those pneumatic tubes you sometimes see on the road) or traffic observers count vehicles for a few days in the year. There is then a fair amount of black magic applied (e.g., Ivan et al. 2002) to arrive at the estimated AADT.

What we are interested in, however, is the Average Daily Traffic (ADT) on an hourly basis. The transportation departments of most major cities collect this data for their major feeder routes, and quite often post the data online. The Province of British Columbia, for example, offers data from a hundred or so traffic counters throughout the province via their Traffic Data Program Web site. Agreed, this is too much information, but it does offer a fascinating insight into urban traffic patterns: they are almost identical on an hourly basis throughout the week, regardless of the city under consideration. A good example is the hourly traffic distribution for all roads in Great Britain in 2014, as reported by the United Kingdom Department for Transport (Fig. 4):

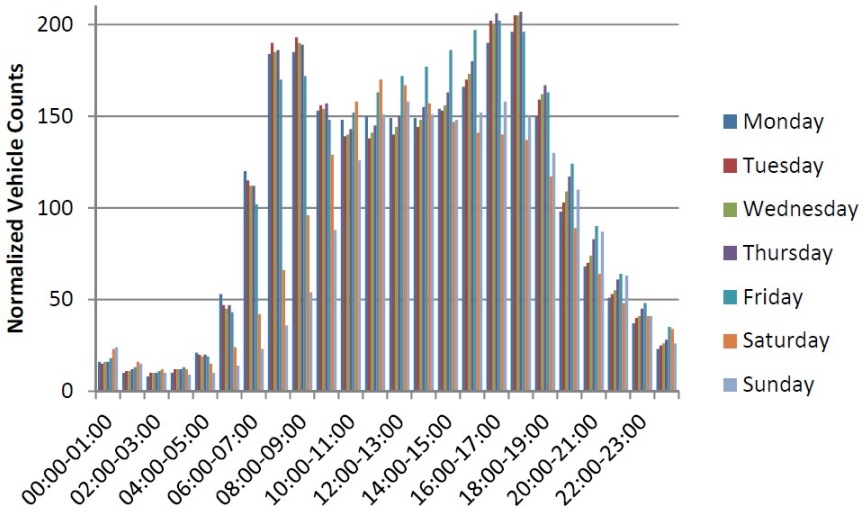

Fig. 4 – Normalized hourly traffic count. (Source: Table TRA0307, UK Department for Transport).

Equally surprising is that these numbers do not change significantly throughout the year (Fig. 5):

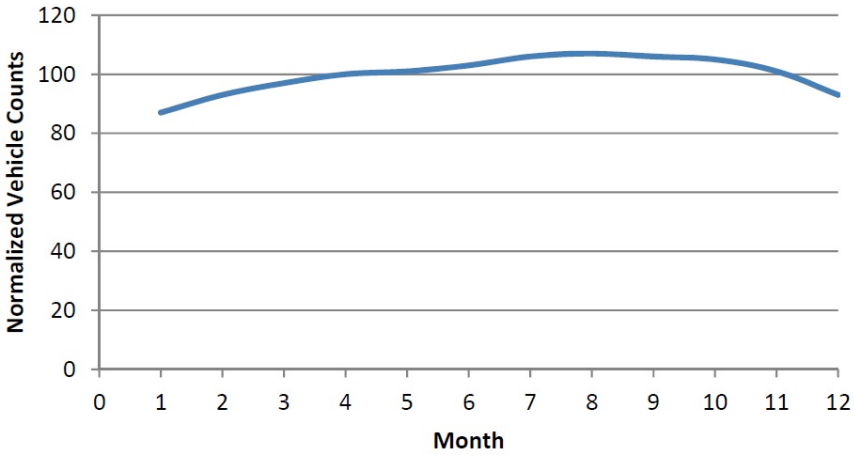

Fig. 5 – Normalized monthly traffic count. (Source: Table TRA0305, UK Department for Transport).

The problem, however, is that these traffic counts apply to single traffic counters. At best, all transportation engineers can do is to monitor the major roads and highways separating different sectors of a major urban center (collectively called "screenlines") and estimate the traffic flow across them. What happens within these sectors with their hundreds to thousands of possible routes along municipal roads is anyone's guess.

So, it is at this point that we have to make some ballpark estimates. We assume (admittedly with no supporting evidence) that the average urban commute time (round trip) per day is two hours, and that 50 percent of the 0.809 vehicles per capita in the United States are driven on any given day. Thus, at any given time, there are *ON AVERAGE* 0.809 * 0.5 * 2 hours / 24 hours = 0.033 vehicles per capita on the road at any given time.

With the normalized hourly traffic counts from Fig. 4 and these data and assumptions, we therefore have:

Hour	Vehicles per Capita	Lumens per Capita
00:00 — 01:00	0.006	36
01:00 — 02:00	0.004	25
02:00 — 03:00	0.003	20
03:00 — 04:00	0.004	23
04:00 — 05:00	0.006	35
05:00 — 06:00	0.013	77

…	…	…
17:00 — 18:00	0.061	367
18:00 — 19:00	0.049	296
19:00 — 20:00	0.035	212
20:00 — 21:00	0.025	152
21:00 — 22:00	0.019	112
22:00 — 23:00	0.014	83
23:00 — 24:00	0.009	56

Table 2 – Automotive lumens per capita and hour

How this table should be interpreted is a matter for debate — it depends on when astronomical twilight begins and ends (i.e., when the sun is 18 degrees below the horizon), and thus on both the time of the year and the observerís latitude. Apart from the winter months, it seems safe to say that automotive headlights contribute less than ten percent to light pollution after astronomical evening twilight.

What happens in San Marino is another question entirely.

Acknowledgements

Thanks to Dawn DeGrazio (Lighting Analysts, Inc.) for reviewing an earlier draft of this article.

References

Aubé, M. 2015. “Physical Behaviour of Anthropogenic Light Propagation into the Nocturnal Environment,” Philosophical Transactions of the Royal Society B 370(1667):20140117.

DOE. 2012. 2010 U.S. Lighting Market Characterization. U.S. Department of Energy Building Technologies Program.

Garstang, R. H. 1986. “Model for Artificial Night-Sky Illumination,” Publications of the Astronomical Society of the Pacific 98:364-375.

Ivan, J. N., W. E. ElDessouki, M. Zhao, and F. Guo. 2002. Estimating Link Traffic Volumes by Month, Day of Week, and Time of Day. Technical Report JHR 02-287, Connecticut Transportation Institute, University of Connecticut.

[1] LED luminaire efficiencies are typically better than their fluorescent and HID counterparts, but these will in general be similar across all applications.

BOTANICAL LIGHT POLLUTION

Ian Ashdown, P. Eng., FIES, Senior Scientist, SunTracker Technologies Ltd. Published: 2016/02/17

Blue-rich light from LED streetlights, we are told, is the nemesis of professional and amateur astronomers. Blue light is preferentially scattered by the atmosphere, resulting in potentially unacceptable levels of light pollution for astronomical observations. Unfortunately, LED streetlights emit more blue light on a per-lumen basis than the high-pressure sodium streetlights they are rapidly replacing.

Botanists and horticulturalists, however, may choose to differ. For them, it is red light from streetlights that is the problem. Depending on the species and various environmental factors, even low levels of light trespass from roadway and outdoor area luminaires can have harmful effects on both wild and domesticated plants. LED streetlights likewise emit more red light on a per-lumen basis than high-pressure sodium streetlights.

This is not a newly discovered problem. Botanists were aware of the deleterious effects of incandescent street lighting on trees eighty years ago (Matske 1936), while horticulturalists became aware of the problem with respect to ornamental plants some forty years ago (Cathey and Campbell 1975).

The lighting community can perhaps be excused for not following the latest research in publications such as American Journal of Botany and Journal of Arboriculture, but we were in fact made aware of the issue through publication of an article in Lighting Design and Application (Cathey and Campbell 1974). However, given that the proposed solution then was to avoid using high-pressure sodium (HPS) lamps and instead use less-efficient mercury-vapor lamps with their ghoulish color rendering capabilities … well, we understandably ignored the advice.

Soybeans and Trees

This is not to say that farmers are not aware of the problem. If you are growing soybeans, you quickly learn not to plant them in a field adjacent to HPS roadway lighting (FIG.1). The nighttime illumination — even as little as two to eight lux — can reduce crop yield by 20 to 40 percent due to delayed flowering and ripening (Chen et al. 2009).

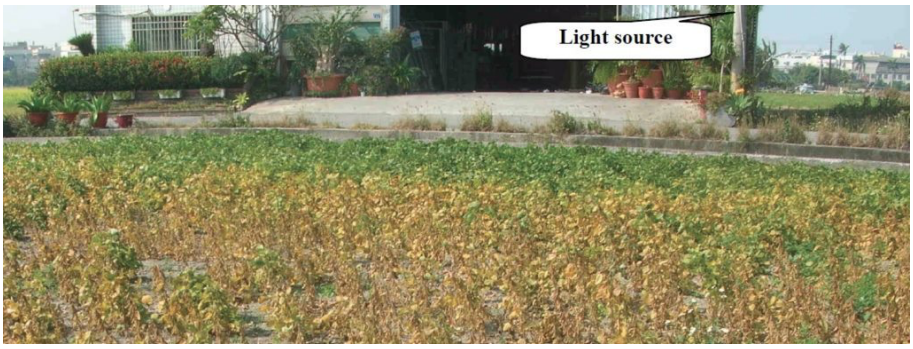

FIG. 1 – Effect of light pollution on soybean crop. (Source: Chen et al. 2009).

Landscape designers and arborists are also aware of the problem. A publication from Purdue University, for example, lists 65 trees and shrubs that are vulnerable to artificial light (Chaney 2002). Exposure to nighttime illumination, particularly from HPS street lighting, may result in disruption of the plant's shoot growth, flowering, leaf expansion and abscission, and bud dormancy. In temperate climates, this may make the plants more susceptible to frost, fungal infections, and insect infestations. Again, however, the advice was to avoid using HPS lighting and use mercury vapor lighting instead. For lighting designers, this is pointless advice — mercury vapor lamps were long ago replaced by high-pressure sodium lamps, and these in turn are being replaced by solid state lighting.

… and herein lies today's issue. LED-based outdoor lighting may — and the emphasis is on the word *MAY* — exacerbate the problem from the perspective of wild and domesticated plants. High-pressure sodium lamps emit much more red light than mercury vapor lamps on a per-lumen basis, and white light LEDs may (depending on their correlated color temperature) emit even more. What was once a minor problem for landscape designers and urban arborists may become something that lighting designers will need to consider.

To better understand this issue, we first need to understand the role of photopigments in plant growth and development.

Phytochrome

Plants perform their magic of photosynthesis using a photopigment called chlorophyll, but this is only one of many different photopigments plants use to harvest and detect light. Equally important is phytochrome, which regulates a long list of plant functions, including:

- Seed germination and development
- Stem elongation

- Leaf expansion and abscission
- Photosynthesis development
- Flowering
- Ripening
- Dormancy

Taken together, these functions basically outline the life cycle from seed to adult plant.
The sum of these light-induced changes is called photomorphogenesis. There are other photopigments involved, including blue light-sensitive cryptochromes (Lin 2002) and ultraviolet-sensitive UVR8 (Goto et al. 2006, Kami et al. 2010). However, it is phytochrome that dominates plant growth and development.

Phytochrome itself is an interesting pigment in that it has two states (or *ISOFORMS*) called P_r and P_{fr} (e.g., Smith 2000). The P_r isoform strongly absorbs red light, with a spectral peak at about 660 nm (FIG. 2), making it look turquoise-blue when dissolved in solution. This is its biologically inactive state.

When a phytochrome molecule absorbs a red photon, it switches to its P_{fr} isoform, making it look slightly more greenish. This is its biologically active state, which signals to the plant that red light has been sensed. While in this state, phytochrome has a different spectral absorption distribution (FIG. 2), with a spectral peak at about 730 nm. (Horticulturalists and plant biologists refer to the spectral range of 700 nm to 800 nm as "far-red," which explains the "fr" subscript.)

When the P_{fr} isoform absorbs a far-red photon, it reverts to its P_r isoform. Thus, phytochrome performs the function of a resettable biological switch to initiate or terminate photomorphological processes.

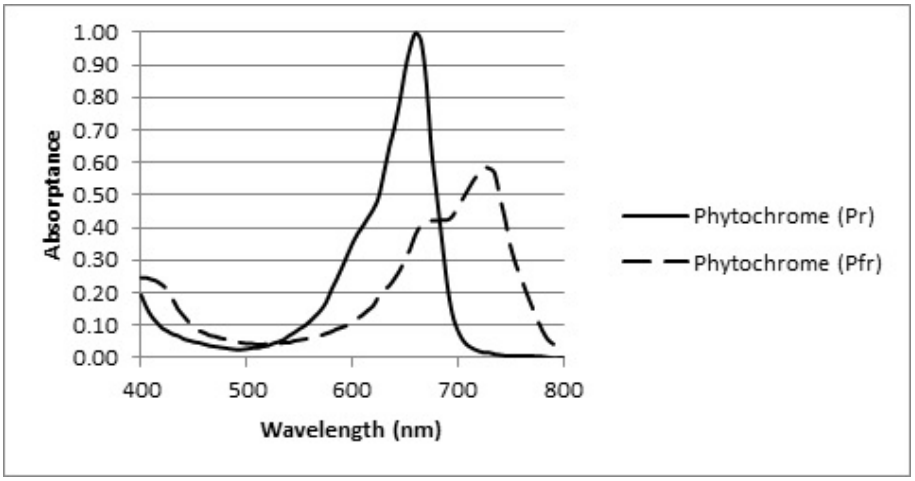

FIG. 2 – Phytochrome absorption spectra. (Source: Plants in Action, First Edition).

This biological switch behavior has some interesting consequences. While even low levels of red light can initiate many physiological responses, applying far-red light soon thereafter may reset the switch and terminate the response. Light pulses as short as one minute at night — think car headlights on a

country road — are enough to induce or prevent the flowering of some plants (Borthwick et al. 1952). Worse, some plants have flower induction thresholds of less than four lux (Botto et al. 1996, Whitman et al. 1998).

Photoperiodism

Phytochrome may act as a biological switch, but how plants respond to its signaling varies by species and even cultivar. What all plants have in common, however, is photoperiodism, their physiological reaction to the length of the day. Like humans and all other animals, plants have circadian rhythms. In terms of flowering, plants can generally be divided into three categories: 1) short day; 2) long day; and 3) day-neutral. For short day plants, flowering is initiated, advanced, or promoted when the dark nighttime period is sufficiently long to allow enough phytochrome P_{fr} to revert to $P_{r.}$ For long day plants, the opposite is true: flowering is initiated, advanced, or promoted when the dark nighttime period is sufficiently short to increase nighttime levels of phytochrome P_r. As for day-neutral plants, their time of flowering is determined by other environmental cues, such as temperature and moisture.

From the perspective of wild and domesticated plants growing outdoors, artificial light can be a problem. For horticulturalists, however, it can be a boon. Florists have long used incandescent lamps with their copious red and infrared emissions to modify the growth and development of flowering plants in greenhouses. This promotes flowering in long day plants such as asters, azaleas, and fuchsias, while delaying flowering in short day plants such as chrysanthemums, begonias, and poinsettias.

The recent availability of high-power red and far-red LEDs has provided new opportunities for both florists and horticulturalists. Independently switching or dimming these LEDs enables greenhouse operators to precisely control phytochrome as a biological switch. This, combined with the secondary effects of activating cryptochromes using blue light, provides remarkable control of plant growth and development (e.g., Gautam et al. 2015, Islam et al. 2014, Kitazaki et al. 2015, and Lee et al. 2015).

Light Pollution

Outside of the greenhouse environment, however, adding red and far-red radiation to the environment is not a good thing. We can call it what it is: botanical light pollution. For soybean farmers and urban arborists, it may be a nuisance. However, there can also be more insidious and detrimental effects for wild plants and the pollinating insects that depend on them (e.g., Bennie et al. 2016).

The question is, how do we quantify this pollution? It is reasonably easy to quantify astronomical light pollution because we have comprehensive mathematical models of atmospheric physics and optics. However, the best that botanists can do for us is to identify plants as short day, long day, or day neutral.

Pragmatically speaking, we do not need to quantify botanical light pollution in an absolute sense of so many micromoles of radiation per square meter per second or whatever. From a lighting design perspective, the goal is to illuminate an area with so many lumens per square meter while doing our best to prevent wasted spill light. The question then becomes, what is the best light source for plants?

Comparing Light Sources

The phytochrome absorptance spectra (FIG. 2) were obtained by extracting phytochrome from plants and dissolving it in solution for analysis *IN VITRO* with a spectrophotometer. When in the plant itself, however, phytochrome is surrounded by other photopigments, especially chlorophyll. Both chlorophyll A and chlorophyll B have absorptance spectra that overlap with those of the phytochrome isoforms (FIG. 3), so it is reasonable to ask whether this influences (or "screens") the phytochrome absorptance spectra *IN VIVO*.

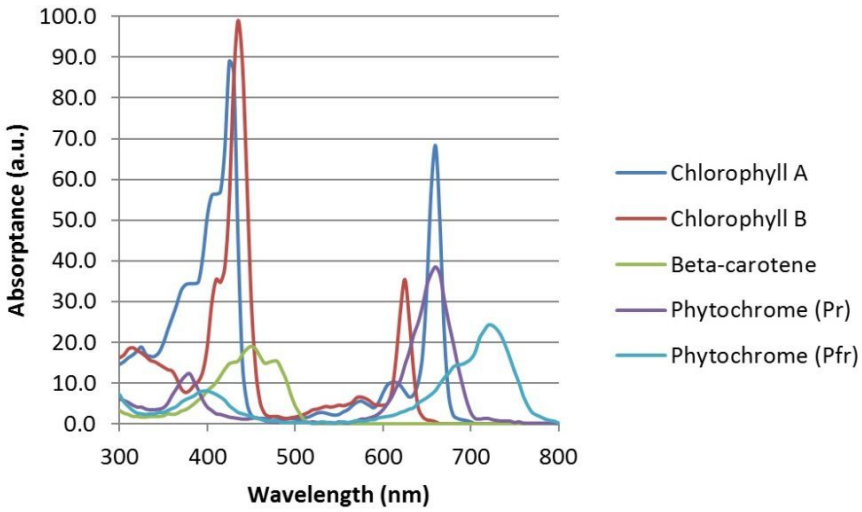

FIG. 3 – Photopigment spectral absorptances.

Fortunately, a variety of studies of the effect of monochromatic radiation on plant growth and development have shown that the absorptance spectra of phytochrome *IN VITRO* reasonably predict the plant physiological response. For example, Withrow et al. (1957) studied the "induction and reversion of hypocotyl hook opening" in bean seedlings. A plot of their results as induction and reversion "action spectra" shows a remarkable correlation with the *IN VITRO* absorptance spectra of phytochrome (FIG. 4).

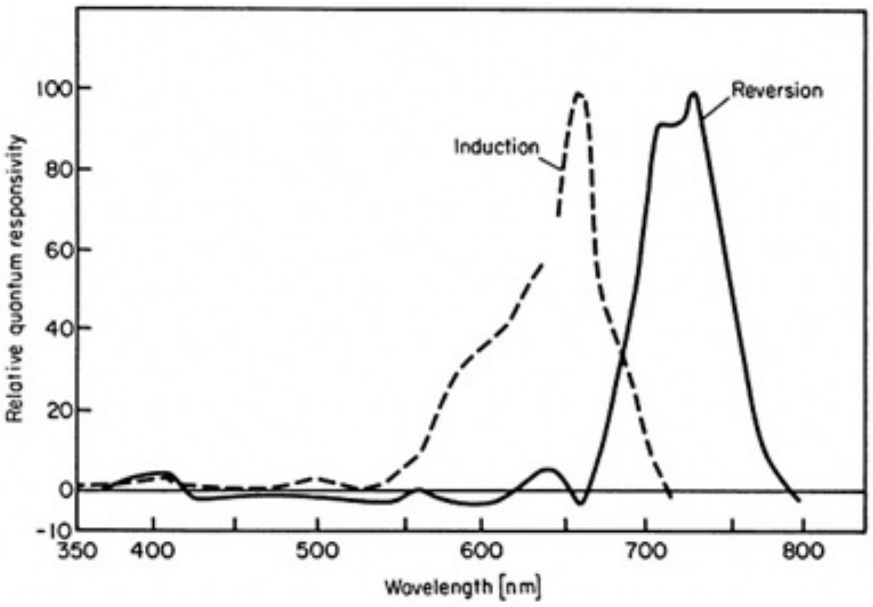

FIG. 4 – Typical phytochrome action spectra. (Source: Smith 1977).

Given this, we can use the phytochrome absorptance spectra as a species-independent measure of the effect of red and far-red radiation on plant growth and development (Sager et al. 1988). For a given light source, the probability of a phytochrome molecule absorbing a photon with a given wavelength is determined by the absorptance spectra of the isoform and the relative number of photons with that wavelength.

For a light source, we typically have its relative spectral power distribution (SPD), which is measured in watts per nanometer. However, from the Planck-Einstein relation, we know that a photon's energy is inversely proportional to its wavelength. Therefore, to determine the relative spectral photon flux distribution, we need only multiply the lamp SPD by the wavelength for each wavelength and normalize the resultant graph. (An example is shown in FIG. 5.)

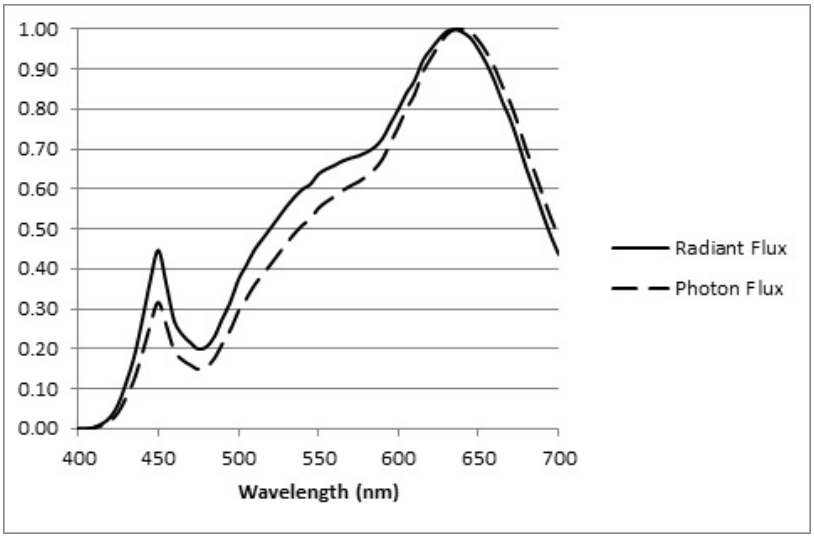

FIG. 5 – Radiant versus photon flux for a 3000K warm white LED.

With this, we now have the means to compare light sources with different spectral power distributions. Given a reference lamp (say, HPS) and a test lamp (say, a 3000K warm white LED), the calculations consist of:

1. Multiply the SPD values of each lamp by the CIE 1931 luminous efficiency function V(λ) shown in FIG. 6 from 400 nm to 700 nm.
2. Sum the results of Step 1 to obtain the relative lumens Φ_{ref} and Φ_{test} generated by the two lamps.
3. Multiply the SPD values of the test lamp by Φ_{ref} / Φ_{test}.

The two SPDs now represent the same number of photopic lumens (i.e., luminous flux) emitted by the lamps. With this:

1. Multiply the SPD values of each lamp by the wavelength to obtain the lamp spectral photon flux distributions from 500 nm to 800 nm.
2. Multiply the results of Step 4 by the phytochrome P_r spectral absorptance spectrum.
3. Sum the results of Step 5 to obtain the P_r action values $PA_{ref,r}$ and $PA_{test,r}$.
4. Multiply the results of Step 4 by the phytochrome P_{fr} spectral absorptance spectrum.
5. Sum the results of Step 7 to obtain the P_{fr} action values $PA_{ref,fr}$ and $PA_{test,fr}$.

and finally:

1. Add the P_r and P_{fr} action values for each lamp to obtain the lamp phytochrome action values PA_{ref} and PA_{test}.
2. Divide PA_{test} by PA_{ref} to obtain the relative action value for the test lamp compared to the reference lamp.

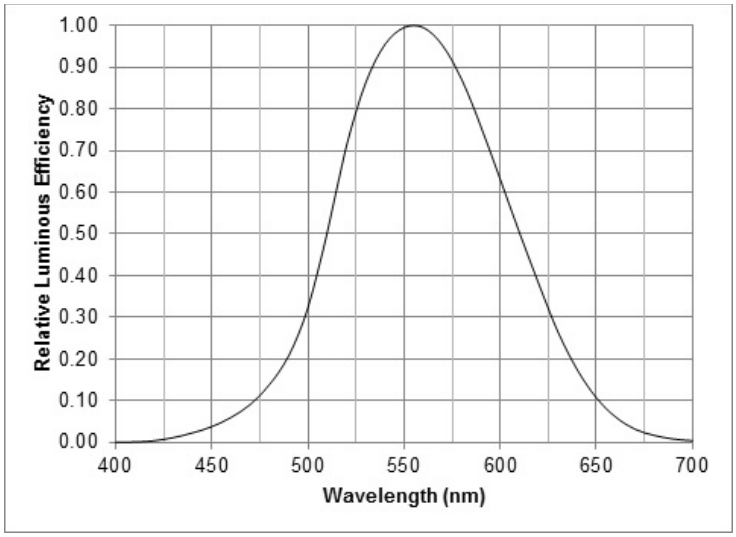

FIG. 6 – CIE 1931 luminous efficiency function V(λ).

A few explanatory notes:

1. As shown in FIG. 2, the phytochrome absorptance spectra have secondary peaks in the near-ultraviolet. These are ignored because: a) it is difficult to disentangle the effects of phytochrome from the effects of the blue-sensitive cryptochrome photopigments; and 2) the photomorphological effects of blue light are less pronounced than those resulting from red and far-red radiation. The lower limit of 500 nm was chosen based on the phytochrome absorptance spectra minima.
2. The spectral peak of P_{fr} is only 60 percent that of P_r, but the area under each spectral curve between 500 nm and 800 nm is almost the same. Also, phytochrome action spectra for various plant species have shown that equal red and far-red radiant fluences at the spectral peaks of 660 nm and 730 nm have approximately equal effect on the physiological responses. This justifies the final step of adding the two action values.

It must be emphasized that these "action values" are approximate at best, and should not be considered as formally quantifiable metrics. They are introduced here only to explore the potential effects of botanical light pollution.

With this caveat then, the following light sources were selected for comparison:

Light Source	Manufacturer Product Code
High-pressure sodium (test)	Damar 1782 LU100M
2700K white light LED	Lumileds LUXEON Rebel ES LXW9-PW27
3000K white light LED	Lumileds LUXEON Rebel ES LXW9-PW30
3500K white light LED	Lumileds LUXEON Rebel ES LXW8-PW35
4000K white light LED	Lumileds LUXEON Rebel ES LXH7-PW40
5000K white light LED	Lumileds LUXEON Rebel ES LXW8-PW40

Table 1 – Comparison light sources.

The HPS lamp SPD was measured in the laboratory with 0.1 nm resolution and averaged to 5 nm bins, while the Lumileds SPDs were digitized from the published datasheet (Lumileds 2014). The equal-lumen SPDs for these light sources are shown in FIG. 7.

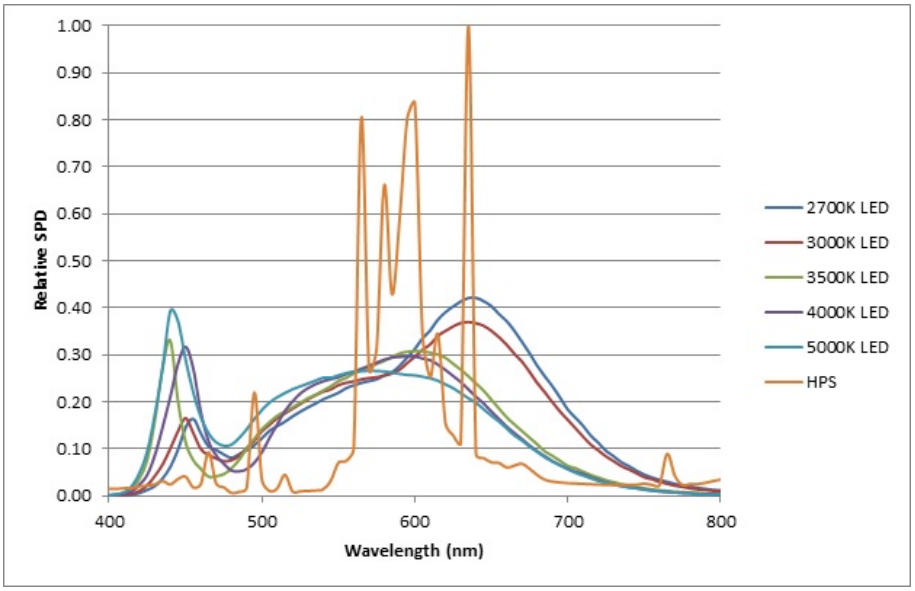

FIG. 7 – Equal-lumen spectral power distributions.

Following the above calculation procedure with the HPS lamp as the test source, the relative phytochrome action values are:

Light Source	Relative Phytochrome Action		
	P_r	P_{fr}	$P_r + P_{fr}$
High-pressure sodium	1.0	1.0	1.0
2700K white light LED	1.7	2.3	1.9
3000K white light LED	1.5	2.0	1.7
3500K white light LED	1.0	1.2	1.1
4000K white light LED	1.0	1.0	1.0
5000K white light LED	0.9	1.0	0.9

Table 2 – Relative phytochrome action values.

From this, it can be seen that while 2700K and 3000K white light LEDs produce the least astronomical light pollution (see related article Color Temperature and Outdoor Lighting), they also unfortunately produce the most botanical light pollution.

It should be noted however that these results apply to Lumileds LUXEON products only. Looking at FIG. 7, it is evident that the 2700K and 3000K products use a different phosphor formulation than the 3500K, 4000K, and 5000K products. Different major LED manufacturers will have their own proprietary phosphor formulations, and so the above results should not be applied to LEDs based solely on their nominal CCTs.

Add More Red

It seems counterintuitive, but one solution to the problem of excess red light generated by low-CCT LEDs is to *ADD MORE RED LIGHT*.

Some of the early LED modules combined phosphor-coated white and red LED dice in order to compensate for the low-efficiency red phosphors then available. This produced a warm white light with good CIE $R_a$values, but relatively poor R9 values due to the quasimonochromatic red emissions. One roadway luminaire manufacturer has recently taken this approach with a new product line that was reportedly designed to comply with the International Dark Sky Association's Fixture Seal of Approval program requirements for a maximum CCT of 3000K. While the approach works (with a measured CCT of 3145K), the massive spike in red light peaking at 625 nm (see Fig. 8) would seem to be a botanist's nightmare spectrum.

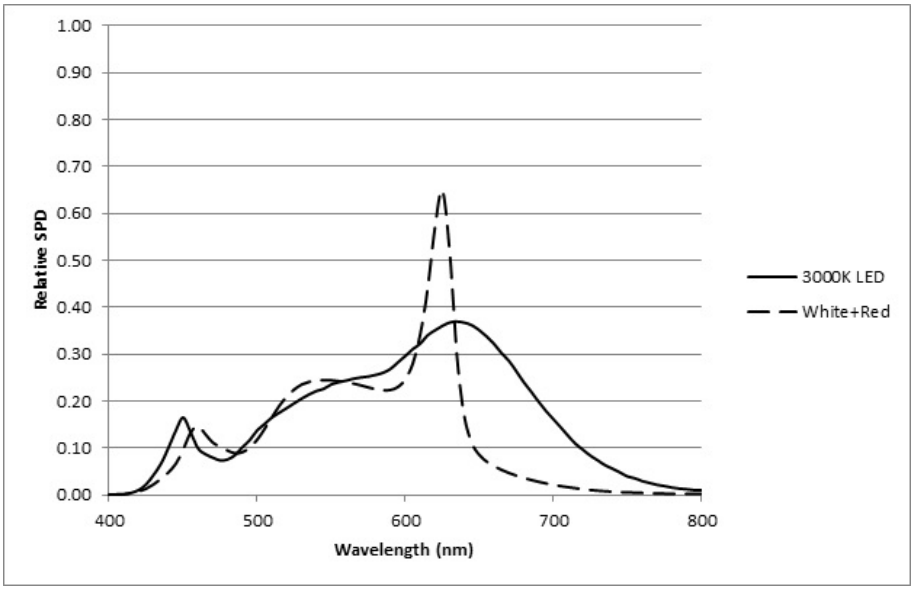

FIG. 8 – 3000K LED versus 3145K white+red LED equal-lumen spectral power distribution.

Surprisingly, the situation may not be as bad as it appears. First, there is relatively little far-red radiation being emitted. Second, the 625 nm peak occurs where the phytochrome P_r absorptance spectrum is only 50 percent of maximum. This results in a calculated phytochrome action value (relative to the HPS reference lamp) of 0.9 — half that of the 3000K LED.

Light Source	Relative Phytochrome Action		
	P_r	P_{fr}	$P_r + P_{fr}$
White+red LED	0.9	0.9	0.9

Table 3 – White+red relative phytochrome action values.

Color Filters

Another solution to the problem of excess red light is simply to add a color filter with a sharp cut-off at 625 nm. Red light beyond the cut-off wavelength contributes only ten percent to the luminous flux of a 3000K white light LED, so it is may be a reasonable trade-off. (The resultant color will, however, be slightly cyan in hue.)

Whether it is possible to develop a suitable dye or coating for the LED optics that is both inexpensive and resistant to fading is, of course, an open question.

Chlorophyll Screening

The preceding analysis necessarily assumes that the phytochrome is not screened by the other plant photopigments, and that the isoform absorptance spectra represent the phytochrome action spectra for any given plant. In practice, this is not necessarily true. Phytochrome is present in very low concentrations in plant tissues. As a result, the much higher concentrations of chlorophyll tend to screen phytochrome by absorbing much of the incident red radiation. (See Fig. 3 for spectral overlapping between phytochrome $P_r$and chlorophyll A.)

A study by Beggs et al. (1980) demonstrated that if mustard seedlings are treated with the herbicide Norflurazon, the chlorophyll in the plant tissue becomes photobleached, resulting in white rather than green seedlings. With white seedlings, the phytochrome action spectrum had a peak at 660 nm, following the phytochrome P_r absorptance spectrum. With untreated green seedlings, however, the action spectrum was shifted to approximately 630 nm — which is well within the range of the 625 nm LED emission of the white+red LEDs (FIG. 9).

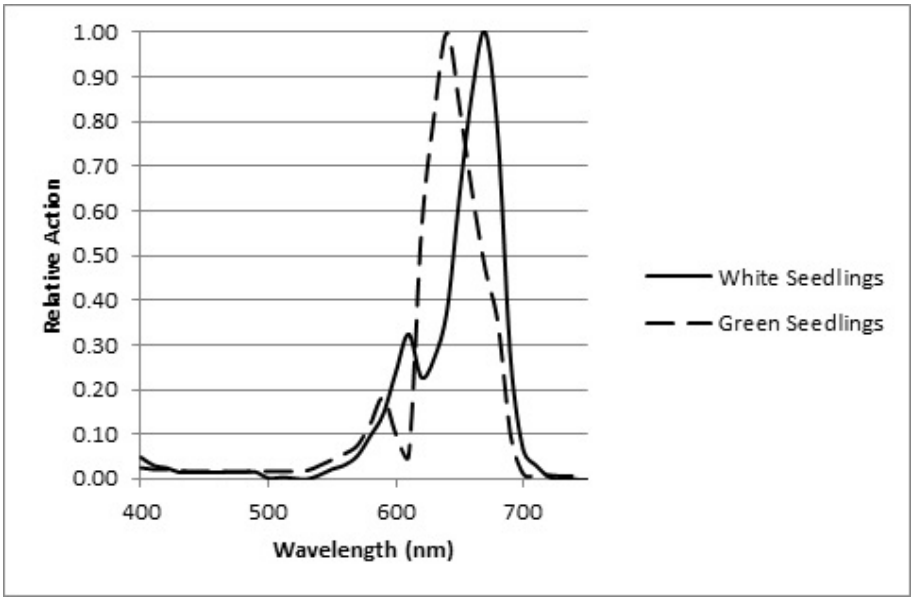

FIG. 9 – Chlorophyll screening of phytochrome Pr action spectrum. (Source: Beggs et al. 1980).

Summary

First and foremost, the phytochrome action metric presented in this article is not intended as a formal light source metric in any sense; it was introduced solely as a means of evaluating the potential impact of red and far-red light on both wild and domestic plants.

Second, the effects of applying red and/or far-red radiation will depend on the physiological state of the plant, the physiological response being mediated, and the time of application. Any excess (i.e., artificial) red radiation will convert the P_r isoform in the exposed plant to P_{fr} , while any excess far-red radiation will convert the P_{fr} isoform to P_r. Either action will upset the plantís *PHYTOCHROME PHOTOSTATIONARY STATE* (Sager et al. 1988). What effect this will have on a given plant species at any given time of the night and season is unknown.

While phytochrome may function as a biological switch for plants, how individual plants species respond to its signaling will vary. Given that phytochrome mediates so many plant functions, the botanist's characterization of short day, long day, and day neutral flowering plants is probably about all they will have in common.

If the above analysis has shown anything, it is that by changing roadway and outdoor area lighting from high-pressure sodium to white light LEDs, we may — and again, the emphasis is on *MAY* — be upsetting the ecological balance in unexpected ways. By examining what we do know and applying it on a theoretical basis, we can at least be better prepared to respond in the future if we need to.

References

Beggs, C. J., M. G. Holmes, M. Jabben, and E. Schafer. 1980. "Action Spectra for the Inhibition of Hypocotyl Growth by Continuous Irradiation in Light and Dark-grown *SINAPIS ALBA* L. Seedlings," Plant Physiology 66:615-618.

Bennie, J. T. W. Davies, D. Cruse, and K. J. Gaston. 2016. "Ecological Effects of Artificial Light on Wild Plants," Journal of Ecology (in press).

Borthwick, H.A., S. B. Hendricks, M. W. Parker, E. H. Toole, and V. K. Toole. 1952. "A Reversible Photoreaction Controlling Seed Germination," Proceedings of the National Academy of Science 38:662-666.

Botto, J. F., R. A. Sanchez, G. C. Whitelam, and J. J. Casal. 1996. "Phytochrome A Mediates the Promotion of Seed Germination by Very Low Fluences of Light and Canopy Shade Light in Arasbidopsis," Plant Physiology 110:439-444.

Cathey, H. M., and L. E. Campbell. 1974. "Lamps and Lighting — A Horticultural View," Lighting Design and Application 4(11):41-52.

Cathey, H. M., and L. E. Campbell. 1975. "Security Lighting and its Impact on the Landscape," Journal of Arboriculture 1(10):181-187.

Chaney, W. R. 2002. Does Night Lighting Harm Trees? Circular FNR-FAQ-17, Department of Forestry and Natural Resources, Purdue University.

Chen, C.-L., Y.-H. Su, C.-J. Liu, and Y.-C. Lee. 2009. "Effect of Night Illumination on Growth and Yield of Soybean," Journal of Taiwan Agricultural Research 58(2):146-154.

Gautam, P., M. T. Terfa, J. E. Olsen, and S. Torre. 2015. "Red and Blue Light Effects on Morphology and Flowering of Petunia x hybrid," Scientia Horticulturae 184:171-178.

Goto, N., T. Kumagai, and M. Koornneef. 2006. "Flowering Responses to Light-breaks in Photomorphogenic Mutants of Arabidopsis thaliana, a Long-day Plant," Physiologia Plantarum 83(2):209-215.

Islam, M. A., D. Tarkowsk·, J. L. Clarke, D.-R. Blystad, H. R. Gislerod, S. Torre, and J. E. Olsen. 2014. "Impact of End-of-day Red and Far-red Light on Plant Morphology and Hormone Physiology of Poinsetta," Scientia Horticulturae 174:77-86.

Kami, C., S. Lorrain, P. Hornitschek, and C. Fankhauser. 2010. "Light-regulated Plant Growth and Development," Current Topics in Developmental Biology 91:29-66.

Kitazaki, K., S. Watanabe, A. Okamoto, M. Matsuo, S. Furuya, and K. Sameshima. 2015. "Far-red Light Enhances Removal of Pericarps in Tartary Buckwheat (*FAGOPYRUM TATARICUM* Gaertn.) Sprout Production under Artificial Lighting," Scientia Horticulturae 185:167-174.

Lee, M.-J., S.-Y. Park, and M.-M. Oh. 2015. "Growth and Cell Division of Lettuce Plants under Various Ratios of Red to Far-red Light-emitting Diodes," Horticulture, Environment, and Biotechnology 56(2):186-194.

Lin, C. 2002. "Blue Light Receptors and Signal Transduction," The Plant Cell 14:S205-S225.

Lumileds. 2014. LUXEON Rebel ES Datasheet DS61 20140630.

Matzke, E. B. 1936. "The Effect of Street Lights in Delaying Leaf-fall in Certain Trees," American Journal of Botany 23(6):446-452.

Sager, J. C., W. O. Smith, J. L. Edwards, and K. L. Cyr. 1988. "Photosynthetic Efficiency and Phytochrome Equilibria Determination Using Spectral Data," Trans. ASAE 31(5):1882-1889.

Smith, H., Ed. 1977. The Molecular Biology of Plant Cells. Berkeley, CA: University of California Press.

Smith, H. 2000. “Phytochromes and Light Signal Perception by Plants — An Emerging Synthesis,” Nature 407:585-591.

Whitman, C.M., R. D. Heins, A. C. Cameron, and W. H. Carlson. 1998. “Lamp Type and Irradiance Level for Daylength Extensions Influence Flowering of Campanula carpatica ‘Blue Clips’, Coreopsis grandiflora ‘Early Sunrise’, and Coreopsis verticillata ‘Moonbeam’,” Journal of the American Society of Horticultural Science 123:802-807.

Withrow, R. B., W. H. Klein, and V. Elstad. 1957. “Action Spectra of Photomorphogenic Induction and its Photoinactivation,” Plant Physiology 32:453-462

[1] *PLANTS IN ACTION* is a plant physiology textbook published by the Australian Society of Plant Scientists, New Zealand Society of Plant Biologists, and the New Zealand Institute of Agricultural and Horticultural Science. It is freely available online at http://plantsinaction.science.uq.edu.au.

FILTERED LEDS AND LIGHT POLLUTION

Ian Ashdown, P. Eng., FIES, Senior Scientist, SunTracker Technologies Ltd. Published: 2016/03/03

6500K Daylight | 2700K Filtered LED | 5000 K Filtered LED

UPDATE 2016/03/03 – Revised Figure 6.

The problem is astronomical — the blue light emitted by LED roadway luminaires has been shown to contribute to light pollution, especially when cool white LEDs are used. Blue light is preferentially scattered by air molecules, and so the higher the correlated color temperature (CCT), the greater the light pollution problem becomes. It is for this reason that the International Dark Sky Association requires a maximum CCT of 3000K for its Fixture Seal of Approval outdoor lighting certification program.

Sometimes, however, even warm white LED street lighting is not enough. For cities that are in close proximity to astronomical observatories, such as Flagstaff, AZ and the nearby US Naval Observatory Flagstaff Station, any amount of blue light is bad news.

Until recently, low-pressure sodium (LPS) street lighting has been the preferred choice. LPS luminaires are ideal light sources in that their monochromatic radiation (590 nm) is easily filtered out for astronomical observations. However, the large physical size of the lamps makes it difficult to control the luminous intensity distributions. For this and other reasons, municipalities are looking at "filtered LED" (FLED) street lighting as an option.

The reasoning is simple: combine a white light LED with a yellow filter and you can eliminate the blue peak that plagues astronomical observations. Figure 1, for example, shows the spectral power distributions (SPDs) of 2700K and 5000K white light LEDs with their characteristic blue peaks, while Figure 2 shows the SPDs of the same LEDs combined with yellow filters. The blue peaks have not been alleviated; they have been completely eliminated.

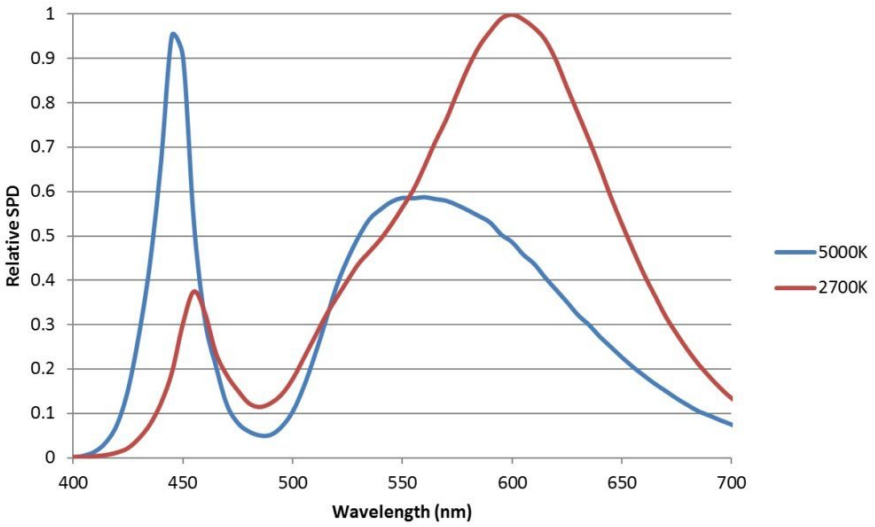

FIG. 1 – White light LED spectral power distributions.

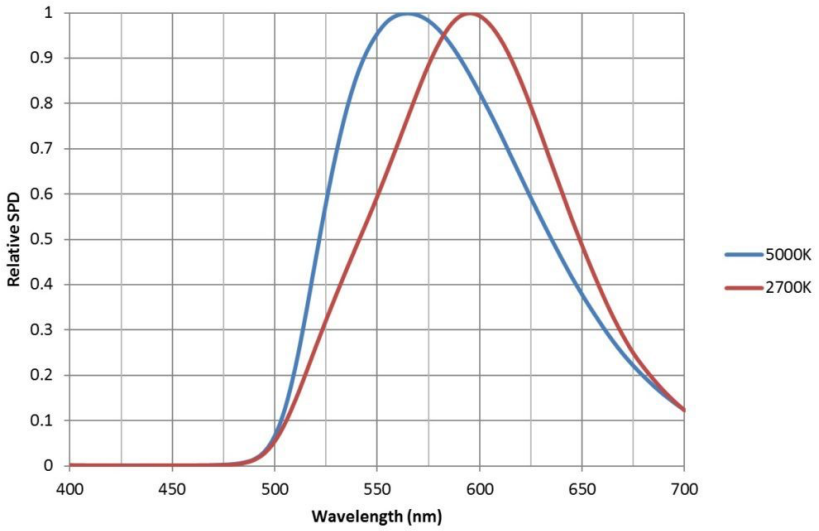

FIG. 2 – Filtered white light LED spectral power distributions.

So, FLEDs are good for astronomical purposes, but what about lighting design?

Luminous Efficacy

At first glance, you might assume that filtering out the blue light will significantly reduce luminous efficacy. Perhaps surprisingly, this is not the case. Based on the SPDs shown in Figure 1 and Figure 2, the loss of luminous efficacy is less than ten percent for both warm white and cool white LEDs,

As a practical example, the SPDs shown in the above figures were taken from the photometric laboratory test reports of two commercial products from CW Energy Solutions. The salient data for these products are:

	WW-CW8-450	CW-CW7-350
Luminaire efficacy (lumens / watt)	106	102
CIE 1931 chromaticity	x = 0.5223 y = 0.4072	x = 0.4719 y = 0.5176
CRI Ra	55.1	38.8
CRI R9	-56.5	-81.9

Table 1 – CW Energy Solution filtered LED roadway luminaire product specifications

To be clear, this is not an endorsement of these commercial products. This information is being provided for educational purposes only.

Chromaticity

We can plot the chromaticity *XY* coordinates shown in Table 1 on a CIE 1931 chromaticity diagram (FIG. 3), but what do the actual colors look like? Unfortunately, most such diagrams reproduce the actual colors of the CIE 1931 color space very poorly. (Worse, it is impossible to display most saturated colors using the RGB color gamut of video displays.)

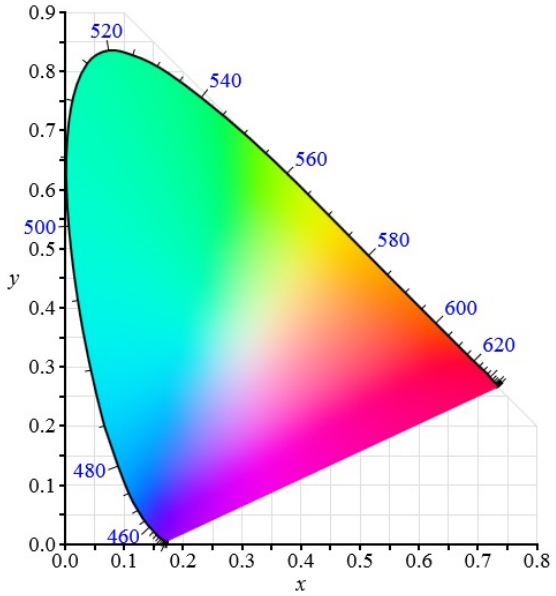

FIG. 3 – CIE 1931 xy chromaticity diagram. (Source: Wikipedia)

To answer this question, we can convert the *XY* chromaticity coordinates into CIE XYZ tristimulus values, and from there, assuming a video display with a 6500K white point, into RGB values for display. The chromaticity coordinates listed in Table 1 then appears much like these colors on a calibrated video display:

FIG. 4A – WWCW8450 light source color.

FIG. 4B – CWCW7350 light source color.

These are clearly not the sort of “white light” luminaires we would normally use for retail or residential lighting … but wait, there is more to this than meets the eye.

Color Rendering Capabilities

Looking again at Table 1, we see that the CIE General Colour Rendering Index Ra values for these products are frankly abysmal — 55 for the filtered 2700k (warm white) LEDs and 38 for the filtered 5000K (cool white) LEDs. The CIE Special Colour Rendering Index R9 values are even worse, with values of -56.5 and -81.9 respectively.

(As a reminder, a CRI value of 100 means that there is no perceptible color shifts with the eight CRI test color samples viewed under the test and reference lamps. It is quite possible, however, to have negative CRI values for the Special CRI values. Low-pressure sodium lamps, for example, have a CRI Ra values of -17.)

It is also interesting, and indeed useful, for lighting designers to understand why these perceived color shifts occur. Johann von Kries, a physiological psychologist who investigated chromatic adaptation in human color vision, noted in 1905 that we tend to see white objects as "white" regardless of the color temperature of the dominant light source. He postulated that our visual system adjusts the "gain" of the signals received from the red-. green- and blue-sensitive cones[1] in our retinae that are responsible for our color vision (von Kries 1905).

von Kries' theory was formalized by the polymath Herbert Ives in 1912 as the von Kries transform, a mathematical operation that forms the basis of the calculation method for the CIE Colour Rendering Indices. While this psychophysiological "gain adjustment" works well (but not perfectly) in enabling us to perceive white surfaces under light sources with different CCTs (e.g., from 2800K incandescent lighting to 8000K overcast daylight), it tends to distort our perception of colored surfaces. (By way of analogy, think of adjusting the bass and treble controls on an audio system — particular settings may work for some music, but be unsuitable for other music.)

The beauty of the von Kries transform, however, is that it enables us to mathematically predict the color shifts due to a given test illuminant. Given a set of test colors — the Gretag-Macbeth ColorChecker is an obvious choice — we can predict *AND DISPLAY* what these colors will look like (e.g., Figure 5).

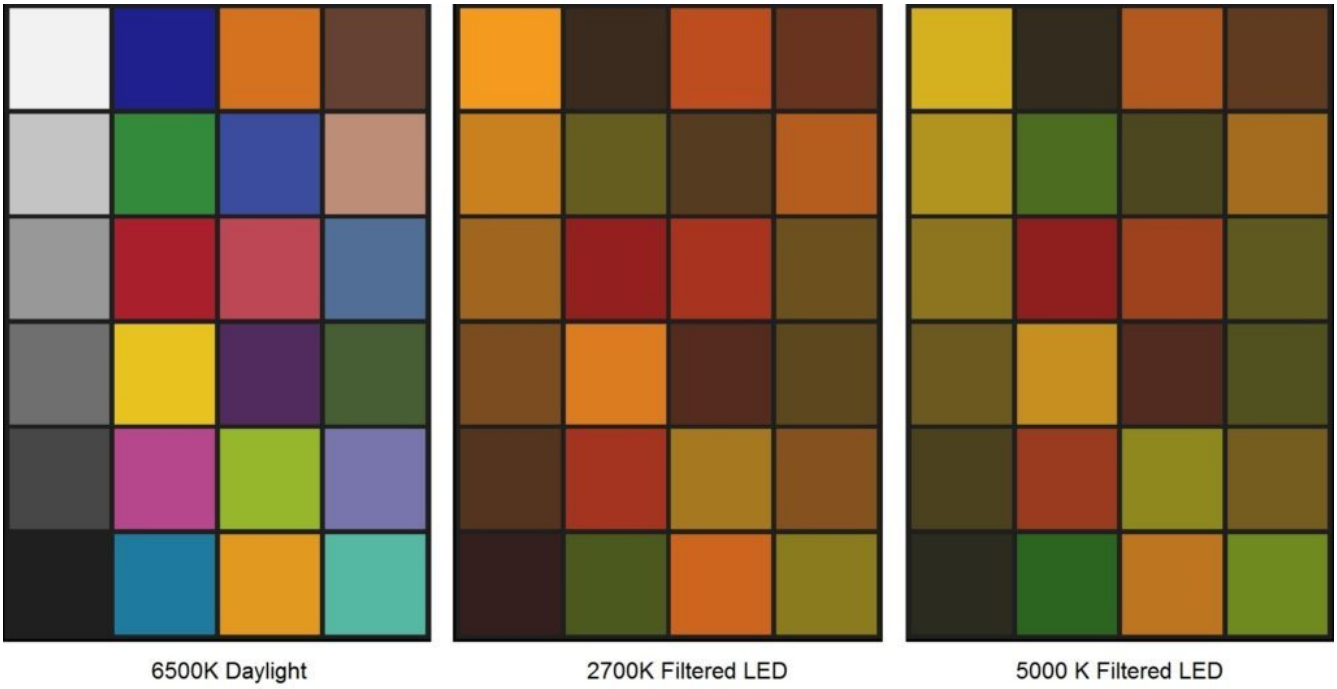

FIG. 5 – Filtered LED color shifts from 6500K daylight.

True — these color shifts are starkly evident, and would be completely unacceptable for retail and residential lighting. However, we need to remember that the topic of discussion is roadway lighting, specifically where municipalities are considering replacing high-pressure sodium (HPS) lamps with LED modules. With this, we need to look at the SPD of a typical HPS lamp (Figure 6).

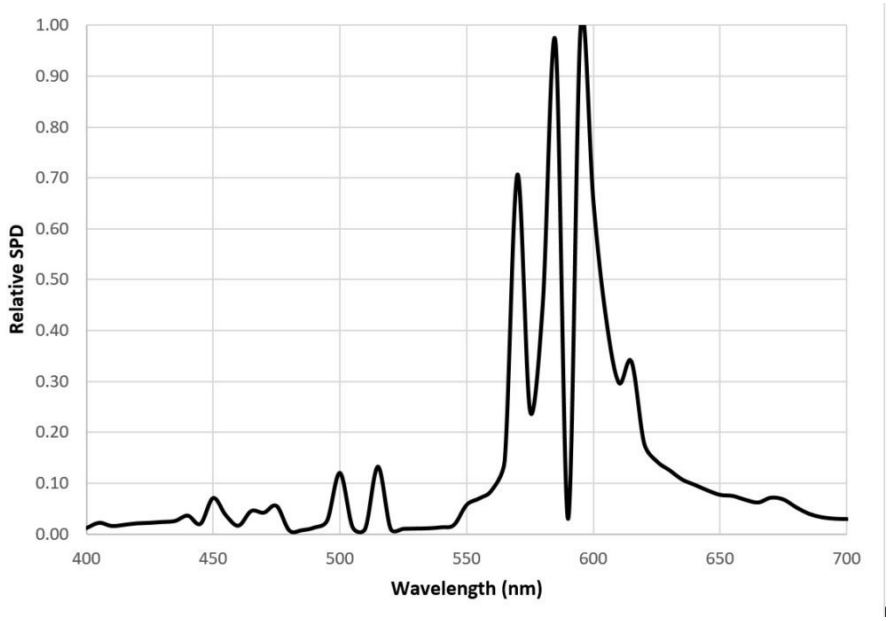

FIG. 6 – 2100K high-pressure sodium lamp spectral power distribution.

There are three points of interest here. First, the correlated color temperature (CCT) rating of 2100K is nominal — the CIE 1931 *XY* chromaticity coordinates of this lamp are not particularly close to the blackbody locus, and so by definition the CCT rating is technically meaningless (CIE 2004).

Second, HPS lamps have a CRI Ra value of 24 — worse than filtered LEDs.

Third – and this is the key point — most municipalities have been using HPS street lighting ever since it replaced the mostly unlamented mercury vapor street lighting in the 1980s. After thirty years of use, most residents have known nothing but their orange-yellow glow.

Putting aside the roadway luminaire manufacturers' arguments that most people prefer "white" light, it is instructive to visualize the color rendering capabilities of filtered LEDs versus HPS lamps (FIG. 7).

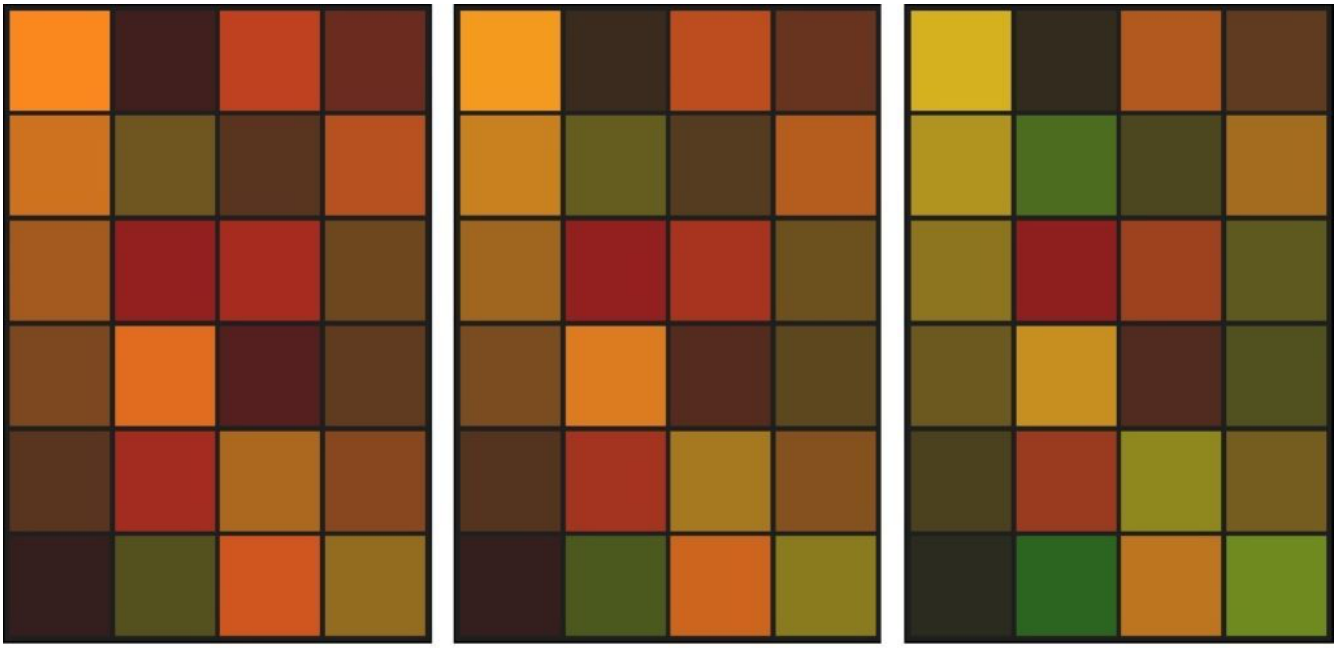

FIG. 7 – Filtered LED color shifts from 2100K daylight.

What is there to say, other than "oh …"? The point is that color rendering under filtered LED illumination is no worse, and arguably somewhat better, than under today's prevalent HPS roadway illumination. It is not the color of the roadway luminaires that is important; it is the *PERCEIVED* colors of the objects that they illuminate.

The deciding factor for most municipalities will likely be whether residents like, dislike, or are simply neutral regarding the color rendering capabilities of filtered LED roadway lighting. In many cases, a test installation will likely be needed. Before then, however, it is important not to dismiss filtered LEDs simply because they are not "white light." Furthermore, it is equally important not to compare them with white light LEDs solely on the basis of their CCT, CRI, or chromaticity values.

Conclusions

The purpose of this article is not to promote filtered LEDs as an alternative to low-pressure sodium lamps, or even as a preferred solution to light pollution problems. Rather, it is an attempt to take the various metrics describing the color rendering qualities of filtered LEDs and visualize them.
How lighting designers, roadway luminaire manufacturers, municipal engineers, and community activists choose to use this information is beyond the scope of this article. All that needs to be said is, "a picture is worth a thousand words."

Acknowledgements

Thanks to Bob Adams of CW Energy Solutions and Tim Robinson of Esterline Corporation for providing the product technical information used in this article.

Thanks to George Livadaras for reporting an error in Figure 6.

References

CIE. 1995. CIE 13.3-1995, Method of Measuring and Specifying Colour Rendering Properties of Light Sources. Vienna, Austria: CIE Central Bureau.

CIE. 2004. CIE 15:2004, Colorimetry, Thirds Edition. Vienna, Austria: CIE Central Bureau.

von Kries, J. 1905. Die Gesichtsempfindungen. Handbuch der Physiologie der Menschen.

[1] These are technically referred to as long-, medium-, and short-wavelength, or LMS, retinal cones.

ALL THINGS LIGHTING® ASSOCIATION

Suite 501 – 747 Fort Street
Victoria, BC Canada, V8W 3E9
www.allthingslighting.org

View this journal at https://www.allthingslighting.org/publications/